Tailoring T_{fh} Profiles Enhances Antibody Persistence to a Clade C HIV-1 Vaccine in Rhesus Macaques

Anil Verma[1*], Chase E Hawes[2,3*], Sonny R Elizaldi[2,4], Justin C. Smith[5], Dhivyaa Rajasundaram[6], Gabriel Kristian Pedersen[7], Xiaoying Shen[8,9], LaTonya D Williams[8,9,10], Georgia D. Tomaras[8,9,10,11], Pamela A. Kozlowski[5], Rama R. Amara[12,13], Smita S. Iyer[1,3,4]

[1]Department of Pathology, School of Medicine, University of Pittsburgh, PA; [2]Graduate Group in Immunology, UC Davis, Davis, CA; [3]California National Primate Research Center, UC Davis, CA; [4]Department of Pathology, Microbiology, and Immunology, School of Veterinary Medicine, UC Davis, CA; [5]Department of Microbiology, Immunology, and Parasitology, Louisiana State University Health Sciences Center, New Orleans, LA; [6]Department of Pediatrics, School of Medicine, University of Pittsburgh, PA;[7] Statens Serum Institut, Copenhagen, DK-2300, Denmark; [8]Duke Human Vaccine Institute, Duke University Medical Center, Durham, NC; Departments of [9]Surgery, [10]Medicine,[11]Molecular Genetics and Microbiology, and Immunology, Duke University Medical Center, Durham, NC; [12]Department of Microbiology and Immunology, Emory University, Atlanta, Georgia, USA; [13] Emory National Primate Research Center, Emory University, Atlanta, GA

*Authors contributed equally

Corresponding author/Lead contact: siyer.3@pitt.edu

ABSTRACT

CD4 T follicular helper cells (T_{fh}) are essential for establishing serological memory and have distinct helper attributes that impact both the quantity and quality of the antibody response. Insights into T_{fh} subsets that promote antibody persistence and functional capacity can critically inform vaccine design. Based on the T_{fh} profiles evoked by the live attenuated measles virus vaccine, renowned for its ability to establish durable humoral immunity, we investigated the potential of a T_{fh}1/17 recall response during the boost phase to enhance persistence of HIV-1 Envelope (Env) antibodies in rhesus macaques. Using a DNA-prime encoding gp160 antigen and T_{fh} polarizing cytokines (interferon protein-10 (IP-10) and interleukin-6 (IL-6)), followed by a gp140 protein boost formulated in a cationic liposome-based adjuvant (CAF01), we successfully generated germinal center (GC) T_{fh}1/17 cells. In contrast, a similar DNA-prime (including IP-10) followed by gp140 formulated with monophosphoryl lipid A (MPLA)+QS-21 adjuvant predominantly induced GC T_{fh}1 cells. While the generation of GC T_{fh}1/17 cells with CAF01 and GC T_{fh}1 cells with MPLA+QS-21 induced comparable peak Env antibodies, the latter group demonstrated significantly greater antibody concentrations at week 8 after final immunization which persisted up to 30 weeks (gp140 IgG ng/ml- MPLA; 5500; CAF01, 2155; $p < 0.05$). Notably, interferon γ+ Env-specific T_{fh} responses were consistently higher with gp140 in MPLA+QS-21 and positively correlated with Env antibody persistence. These findings suggest that vaccine platforms maximizing GC T_{fh}1 induction promote persistent Env antibodies, important for protective immunity against HIV.

INTRODUCTION

Despite options for testing and treatment, progress against HIV is slowing, emphasizing the urgent need for an HIV vaccine (Fauci 2017, Eisinger and Fauci 2018). While advances have been made in immunogen design and vaccine approaches, the main challenge lies in generating durable, high-affinity antibodies against the HIV-1 Envelope (Env) glycoprotein, crucial for protection. To design a vaccine that confers long-term protective immunity, effective stimulation of CD4 T follicular helper (T_{fh}) cells is essential, as they provide vital costimulatory and cytokine support to B cells within germinal centers (GC), leading to the production of persistent antibodies following immunization (Slifka, Antia et al. 1998, Crotty 2014). T_{fh} cells possess distinctive T_h1, T_h2, and T_h17-type cell attributes, programmed by the inflammatory response during the T-cell priming phase, with each T_{fh} subset differentially contributing to GC B cell proliferation, survival, and differentiation (Morita, Schmitt et al. 2011, Barbet, Sander et al. 2018) (Gao, Luo et al. 2023). Therefore, in addition to antigen selection, promoting the differentiation and expansion of optimal T_{fh} subsets to generate potent and enduring humoral immunity is critical for vaccine design.

Clinical studies have demonstrated that booster immunization with a T_h1 glucopyranosyl lipid adjuvant-stable emulsion (GLA-SE)-formulated malaria antigen leads to enhanced antibodies at memory time points compared to an aluminum adjuvanted vaccine (Hill, Pierson et al. 2019). We demonstrated that promoting the induction of $T_{fh}1$ cells by utilizing interferon-induced protein (IP)10, a ligand for and an inducer of CXCR3, as a molecular adjuvant to a DNA vaccine (DNA_{IP10}) followed by boosting with protein adjuvanted with Army Liposome Formulation (ALFQ) consisting of liposomal monophosphoryl lipid A (MPLA) plus a saponin derivative, QS-21 (Alving, Peachman et al. 2012, Rao, Onkar et al. 2018) enhanced GC responses, increased HIV anti-Env binding antibodies, and stimulated significantly higher cross-clade reactivity with

increased specificity to V1V2 conformational epitopes, and higher avidity (Verma, Schmidt et al. 2019). Similarly, a recent macaque study utilizing Clade C DNA+GLA-SE adjuvanted Env protein immunization revealed that frequencies of Env-specific CD28+ IFNγ+ cells, indicative of T_h1 responses, correlated with the development of Env antibodies following the final immunization (Felber, Lu et al. 2020).

In addition to IFNγ, interleukin 17 (IL-17) has been shown to enhance cognate T-B cell interactions, leading to an effective GC response (Moyron-Quiroz, Rangel-Moreno et al. 2004, Mitsdoerffer, Lee et al. 2010, Kumar, Chen et al. 2013). Studies conducted in mice have further demonstrated that $T_{fh}17$ cells support efficient antibody recall responses (Gao, Luo et al. 2023). Notably, the persistence of circulating $T_{fh}17$ cells specific to measles has been observed in adults who have received the live attenuated measles virus vaccine (LAMV) during childhood, suggesting that measles vaccine triggers $T_{fh}17$ responses which persist beyond the GC phase (Gao, Luo et al. 2023). Intriguingly, earlier studies exploring peripheral CD4 T cell determinants of serological memory elicited by LAMV have led to the hypothesis that LAMV promotes both T_h1 and T_h2 CD4 differentiation programs, based on production of IFNγ$^+$ and IL-4, which are cytokines also produced by T_{fh} cells (Ovsyannikova, Dhiman et al. 2003) (Ward and Griffin 1993, Ovsyannikova, Reid et al. 2003). However, our understanding of the GC T_{fh} cell response to LAMV, which plays a crucial role in establishing long-term immunity against measles, remains incomplete.

In this study, based on GC T_{fh} profiles evoked by LAMV, we explored the potential of a $T_{fh}1$ or mixed $T_{fh}1/17$ targeted vaccine to enhance HIV-1 Env antibodies in rhesus macaques using an DNA-prime/protein boost approach. After booster immunization with a Clade C gp140 protein formulated in CAF01 (Wørzner, Hvannastein et al. 2021), a cationic liposome-based formulation, we observed the generation of $T_{fh}1/17$ cells within GCs, while $T_{fh}1$ cells were

induced when MPLA+QS-21 was used as the adjuvant. Notably, stimulating $T_{fh}1$ cell induction with MPLA resulted in significantly greater antibody persistence at week 8 and up to 30 weeks after the final immunization. Moreover, the $T_{fh}1$ regimen with MPLA adjuvant led to higher tier 1 neutralization titers, increased levels of IgG1 subclass antibodies, and improved antibody effector functions. These findings highlight a unique potential of $T_{fh}1$ cells in promoting humoral immunity against HIV and suggest that vaccine strategies maximizing $T_{fh}1$ cell induction may hold promise for eliciting durable protective immunity against HIV.

RESULTS

GC $T_{fh}1$ and GC $T_{fh}17$ cells recalled by measles booster.

To decipher the specific T_h subset of T_{fh} cells contributing to the establishment of durable serological memory, we employed live attenuated measles virus vaccine (LAMV) as a model and investigated T_{fh} responses in peripheral blood and lymph nodes (LN) in a cohort of 16 healthy adult female rhesus macaques (**Figure 1A**). Consistent with documented evidence of long-term persistence of the memory B cell response to LAMV, rapid recall of measles virus (MeV) IgG ensued at week 2 post LAMV, irrespective of the booster interval (**Figure 1B**). By week 20, MeV IgG concentrations displayed a 2.6-fold increase compared to baseline, signifying the efficacy of LAMV booster in generating persistent antibodies. These augmented levels of memory antibodies were accompanied by enhanced antibody avidity (**Figure 1C)**, underscoring robustness of the humoral immune response elicited by LAMV.

Tracking MeV-specific T_{fh} cells using the activation-induced marker (AIM) assay showed induction of circulating (c)T_{fh} cells at day 7 post-vaccination (**Supplementary Figure 1A**). Confirming T_{fh} cell induction in response to LAMV, activated cTfh cells, identified by co-expression of ICOS and Ki-67, were transiently upregulated at day 7 (**Fig 1D, Supplementary Figure 1B**). These responding cTfh cells were PD-1+ and their frequencies at day 7, but not day 0, significantly correlated with MeV IgG at Week 20 (**Fig 1E**). We next proceeded to analyze heterogeneity within cTfh cells with respect to expression of T_h1/2/17 chemokine receptors. Our temporal analysis of the responding cTfh compartment demonstrated significant induction of CXCR3+ T_{fh}1 cells at day 7 (**Fig 1F**). In contrast, we observed a decrease in frequencies of CCR4-expressing cTfh2 subsets and CCR6-expressing cTfh17 subsets. Utilizing Boolean

analysis, we further identified that the majority of responding cTfh cells expressed CXCR3, indicating induction of cTfh1 cells in response to LAMV (**Fig 1G**).

Expanding our investigation to include phenotypic and molecular features of CXCR5^{+} PD-1^{++} GC T_{fh} cells (**Fig 1H, Supplementary Figure 1C),** we found that of the GC T_{fh} cells expressing either CXCR3 or CCR6, CXCR3 expression predominated (median %CXCR3+, 28%). Additionally, we observed that on average 7% of GC T_{fh} cells expressed CCR6. Notably, our analysis did not reveal substantial expression of CCR4 within GC T_{fh} cells (**Fig 1I**). Molecular analysis of sorted CXCR5+ PD-1+/++ LN T_{fh} cells (**Supplementary Figure 1D**) further provided insights into their functional specialization, with the induction of key transcription factors BATF and IRF4, as well as the expression of chemokine receptors CCR5 and CCR6, indicating the activation of T_h1 and T_h17 programs within GC T_{fh} cells (**Figure 1J-K**). Collectively, these findings demonstrate that both blood and GC T_{fh} cells, during the peak effector response following LAMV immunization, exhibit a predominant T_{fh}1 helper bias, with GC T_{fh} cells also demonstrating a T_{fh}17 bias.

HIV-1 vaccine modalities for inducing GC T_{fh}1 and GC T_{fh}17 subsets.

Building on our observations made with LAMV, we next investigated the potential of fine-tuning T_{fh} responses towards T_{fh}1 and T_{fh}17 profiles for generation of persistent anti-HIV-1 Env antibodies. We immunized two cohorts of rhesus macaques against HIV Env using a DNA prime and protein boost vaccination strategy tailored towards either a T_{fh}1 (n=6) or mixed T_{fh}1/17 (n=6) response (**Supplementary Figure 2**). For both vaccine regimens, animals received an initial intradermal DNA prime vaccine encoding HIV-1 Env gp160 (C.1086C) at weeks 0, 4, 8, followed by an subcutaneous HIV C.ZA 1197MB Env gp140 protein boost vaccination at weeks 12 and 20. To tailor vaccine induced T_{fh} responses, we included additional T_{fh} polarizing factors with DNA prime vaccines encoding for cytokines IP-10 (T_{fh}1 regimen) or IP-10 and IL-6 (mixed

T_{fh}1/17 regimen), coupled with corresponding gp140 protein boost formulated in either the T_h1 polarizing adjuvants, MPLA+QS-21, or the T_h1/17 polarizing CAF01 adjuvant platform, respectively. Over the course of both the priming and boost stages, we performed routine collection of both blood and rectal secretions from animals to assess the extent of systemic and mucosal humoral immunity elicited by the two regimens. Additionally, we collected inguinal LN biopsies and fine needle aspirates of LN (FNA) at baseline, during the DNA prime stage, and following both protein boost to comprehensively characterize vaccine-elicited GC T_{fh} responses in draining LNs. GC responses typically peak between 2-3 weeks post first booster with more rapid recall kinetics after the second booster (Iyer, Gangadhara et al. 2015). Our rationale for sampling LN 3 weeks following the 2nd booster was to assess whether the reported effects of CAF01 on sustained antigen release might result in GC persistence (Henriksen-Lacey, Christensen et al. 2011, Pedersen, Wørzner et al. 2020).

Induction of Robust T Cell Activation in GCs with HIV-1 Env Formulated in CAF01 and MPLA+QS-21 Adjuvants.

To gain insights into LN T_{fh} responses induced by MPLA and CAF01 platforms, we utilized complementary approaches of in-situ protein expression analysis of GCs and RNA sequencing of Env-stimulated CD95+ CD4 T cells of selected animals in each vaccine group (**Figure 2A**).To track immunological changes within GCs, we applied the GeoMx Digital Spatial Profiler to assess protein expression of key immune targets longitudinally at baseline (BL, prior to DNA immunization), week 2 post-protein 1 (P1w2) and week 3 post-protein 2 (P2w3) immunizations. We stained tissue sections with morphological markers (CD20, CD3, Ki-67) and collected circular regions of interest (ROI) based on co-localization of CD3 with CD20+ Ki-67+ GC B cells. For each tissue, two to three ROIs were selected to ensure adequate representation of GCs within each animal. This approach allowed us to accurately identify GCs and analyze protein expression of both T and B cells within these specific regions (**Figure 2B**).

Thirty-two protein targets were profiled simultaneously, along with isotype controls (Ms IgG1, Ms IgG2A, Rb IgG) and housekeeping proteins (S6, Histone H3, GAPDH). After applying quality control measures, we calculated the signal-to-noise ratio for each target which provided robust assessment of protein expression levels (**Supplementary Figure 3A-D**). CD45 and B2M were among the most abundantly expressed proteins while LAG3 and PD-L1 demonstrated low signal expression. To address variations in ROI surface area and tissue quality, normalized protein expression (NPE) was calculated for each protein. NPE analysis revealed robust expression of key lineage proteins, CD45, CD20, CD3, CD4, and CD8, as well as GC markers PD-1 and Ki-67 within ROIs (**Figure 2C**). We observed notable associations between protein expression patterns within the GC microenvironment; specifically, a strong correlation between the expression of CD4 and CD20 was observed (**Supplementary Figure 3E**). Furthermore, a significant association between the co-stimulatory molecule 4-1BB and CD4 expression (**Supplementary Figure 3F**) was observed within the GC. Association of the innate immune protein stimulator of interferon genes (STING) with both 4-1BB and CD4 expression suggested a potential interplay between innate and adaptive immune pathways within the context of GC responses. Altogether, the protein expression data provide evidence for coordinated expression of key proteins involved in GC function in both vaccine groups (**Supplementary Figure 3G)**.

To identify specific proteins and pathways activated in response to vaccination, we performed differential expression analysis on a per-protein basis. We modeled NPE using a linear mixed-effect model (LMM), which allowed us to account for sampling multiple ROIs per tissue within each animal (FDR p value cut-off, < 0.05). Volcano plots illustrate proteins induced at P1w2 (**Figure 2D**) and P2w3 (**Figure 2E**) following vaccination. Induction of 4-1BB, ICOS, PD-1, CD44 post boost indicated activation of T cells to antigen stimulation within GCs in both vaccine groups (**Figure 2F**). The higher relative expression of these proteins at P2w3 was

consistent with the reported effects of CAF01 in GC persistence. We found that expression of the checkpoint inhibitors CTLA4 and PD-L1 was significantly reduced post CAF01 vaccination, while CD4 expression increased. In contrast, expression of the regulatory enzyme, IDO1; checkpoint inhibitor, PD-L2; and CD256 (B7-H3), and the innate sensor, STING, was significantly higher post vaccination in the MPLA group (**Figure 2D-E, G**).

Across vaccine regimens, significant differences were observed at P1w2 (**Figure 2H**). Significantly higher expression of Ki-67 with MPLA compared to CAF01 was suggestive of a more rapid GC response (**Figure 2H**). Furthermore, the checkpoint inhibitory receptors LAG3, CTLA4, as well as IDO1, exhibited higher expression levels with MPLA at P1w2. Importantly, no significant differences were observed at BL, validating the specificity of immune activation to vaccination. Altogether, the in-situ protein analysis indicated robust induction of GC responses across vaccine platforms with distinct qualitative and quantitative effects initiated by MPLA versus CAF01 suggesting potential differences in regulatory mechanisms and immune activation pathways between the vaccine regimens.

T_h1 molecular programs potentiated by HIV-1 Env/MPLA+QS-21.

To assess the extent of T_h1/T_h17 programming in CD4 T cells induced by vaccination, we profiled the transcriptome of CD95+ CD4 T cells isolated from the LN. We sort purified and RNA sequenced naive (CD95-) and CD95+ CD4 T cells at BL, P1w2, and P2w3 following overnight stimulation with HIV-1 Clade C Env peptide pools. A total of 18 samples per group, which included three biological replicates per subset, were sequenced in parallel resulting in over 25 million high-quality reads per sample (**Figures 3A, Supplementary Figure S4A-B**). The transcriptomes of naive versus CD95+ CD4 T cells post immunization, in alignment with their distinctive biological states, exhibited clear demarcations along distinct dimensions within the principal component analysis (PCA) plot (**Figure 3B**). Transcription factors (TF) involved

in regulating distinct cellular differentiation programs were enriched in CD95+ CD4 T cells at P1w2 and P2w3. These included HOPX, IKZF2, PRDM1, RUNX2, associated with effector differentiation. Additionally, TF such as BATF, BCL6, BHLHE40, EGR2, and TOX2 involved in T_{fh} differentiation were also identified. Furthermore, we identified genes regulating T_h1 (STAT1, TBX21, EOMES), T_h17 (AHR), and Treg (FOXP3, NR4A2) programs. Moreover, the expression of interferon regulatory factors (IRFs) controlling T cell differentiation (IRF1, IRF5, IRF8) was observed, demonstrating that CD95+ cells post vaccination encompassed effector and fully differentiated CD4 T cell subsets (**Figure 3C**).

We first assessed temporal changes in gene expression by focusing on differentially expressed genes (DEGs) within CD95+ cells at P1w2 and P2w3, compared to BL (**Venn diagram in 3D**). Notably, a significantly higher level of transcriptional perturbation was observed in response to CAF01, particularly at P2w3, within both naive and CD95+ CD4 T cells (**top bubble plot in 3D, Supplementary Figure S4C**), suggesting that CAF01 induces extensive gene expression changes in a cell-extrinsic manner. By specifically examining genes induced exclusively in CD95+ cells, but not naive cells, at P1w2, we made several observations. The T_h1 transcriptional regulator STAT1, as well as IFNγ-induced genes such as IRF7, IRF8, IFI30, XAF-1, and CXCL11, were among the most highly expressed genes in MPLA (**bottom bubble plot, 3D**), highlighting the activation of T_h1 programs following vaccination. Indeed, interrogation of top 3 enriched pathways utilizing the Reactome database (Fabregat, Sidiropoulos et al. 2017) revealed that genes encompassing IFNγ, IL-7, and IL-10 signaling networks were induced with MPLA at P1w2. In the CAF01 group, we observed enrichment of co-stimulatory molecules TNFRSF8 (CD30) and TNFRS13B (TACI), expressed by activated T cells, along with expression of the anti-apoptotic molecule BCL-2 and the transcription factor Foxp3.

Analysis of genes downregulated showed pathways regulating cell cycle inhibitors p21 and p53 were enriched with MPLA while pathways regulating cellular responses to stimuli and stress were downregulated with CAF01 (**Figure 3E**). Collectively, transcriptional profiles demonstrated activation of effector programs within CD4 T cells with common and unique pathways induced across vaccine platforms.

Consistent with this, $CD95^+$ CD4 T cells at P1w2 and P2w3 exhibited notable clustering patterns across vaccine regimens. Particularly, tighter, and more distinct clusters were observed at P1w2 compared to P2w3 notably with CAF01 (**Figures 3F, Supplementary Figure 4D-E**). Exploration of genes regulating T_h1 and T_h17 programs within CD95+ CD4 T cells at P1w2 showed that CD95+ CD4 T cells in both MPLA and CAF01 groups exhibited overlapping expression profiles, with genes regulating major classes of cytokine-cytokine receptor interactions represented. The MPLA group exhibited higher expression levels of IFN-induced chemokines CXCL10 and CXCL11, IL1 family members IL18 and IL1RAP, IL15 family members IL15 and IL15RA, as well as TNF cytokine family members FAS, TNFα, TNFRSF8 (CD30), and TNFRSF9 (4-1BB) (**Figure 3G-H, Supplementary Figure 4F**).

In contrast, the CAF01 group demonstrated expression of the T_h17 receptor IL23R, along with TNF family members FASLG, TNFRSF13B (TACI), TNFRSF11 (RANKL), and TNFRSF12 (DR3) within CD95+ cells with higher relative expression of IL17A observed with CAF01, indicative of T_h17 responses (**Figure 3I, Supplementary Figure 4G**). Collectively, this gene-level analysis indicated strong engagement of T_h1 molecular programs within LN CD4 T cells with MPLA.

Phenotypically and functionally specialized GC $T_{fh}1$ / $T_{fh}17$ subsets elicited with HIV-1 Env Formulated in CAF01 and MPLA+QS-21 Adjuvants.

After confirming the robust induction of GC responses by both vaccines and observing distinct molecular programs in CD4 T cells, we proceeded to investigate the phenotypic and functional characteristics of T_{fh} cells. We examined the GC T_{fh} cell subset characterized by the expression of CXCR5 and high levels of PD-1, using the gating strategy outlined in **Supplementary Figure 5A.** Our analysis of the lymph nodes revealed an increase in the frequencies of GC T_{fh} cells following each protein boost in both groups compared to baseline. Importantly, there were no statistically significant differences observed between the two adjuvant platforms, as shown in **Figure 4A**. We further examined the frequencies of T_{fh} cells characterized by the expression of CXCR5 and PD-1 (CXCR5+ PD-1+), which also exhibited a significant increase following the first protein boost in both groups (**Supplementary Figure 5B**).

To gain insights into the T_{fh} helper profiles within the GC, we assessed the expression of CXCR3 ($T_{fh}1$) and CCR6 ($T_{fh}17$) on the GC T_{fh} cells (**flow plot in B)**. Both adjuvants induced GC $T_{fh}1$ cells, as evidenced by the expression of CXCR3. However, a selective increase in GC $T_{fh}1/17$ cells was observed with CAF01, while the frequencies of GC $T_{fh}17$ cells did not show a significant increase following immunization (**Figure 4C)**.

At P1w2, our investigation into the relative frequencies of polarized GC T_{fh} subsets revealed significant insights. We observed that most GC T_{fh} cells retained a non-polarized state (with respect to expression of CXCR3 and CCR6), with no substantial distinctions noted between the CAF01 and MPLA groups. Notably, the T_h1 GC subset demonstrated a significant increase in the MPLA group, while the T_h17 subset exhibited a higher prevalence in the CAF01 group (**Figure 4D)**. This observation was further supported by Boolean analysis, which revealed a greater proportion of the T_h17 subset associated with CAF01, and a higher proportion of the GC $T_{fh}1$ subset with MPLA at P1w2, as illustrated in **Figure 4E**.

Following the observed induction of LN $T_{fh}1$ responses, we quantified the Env-specific CD4 T cell response using intracellular cytokine staining (ICS). The analysis revealed higher relative frequencies of Env-specific T_{fh} cells and Env-specific CXCR5- CD4 T cells producing IFNγ with MPLA compared to CAF01 **(Supplementary Figure 5C**). To obtain a more comprehensive understanding of the cytokine profile within the LN $T_{fh}1$ and $T_{fh}17$ subsets, we assessed cytokine production after PMA/Ionomycin stimulation (**Figure 4F**). By utilizing the discrete expression patterns of CXCR3 and CCR6 on CXCR5+ CD4 T cells in the LN, in conjunction with the canonical cytokines IFNγ (T_h1), IL-17 (T_h17), and IL-21 (T_{fh}), we made several important observations. Firstly, we found that within the $T_{fh}1$ subset, IL-21+ IFNγ+ co-producing cells were more abundant, and their levels were significantly increased with MPLA stimulation (**Figure 4G**). Conversely, within the $T_{fh}17$ subset, we observed that IL-21+ IL-17+ co-producing cells were more abundant, and their levels were significantly higher in the CAF01 group. Notably, the $T_{fh}1/17$ subset demonstrated the highest degree of polyfunctionality, as evidenced by the production of multiple cytokines.

We further analyzed the cytokine profiles by gating IFNγ and IL-21 co-producers versus IL-21 single producers. This analysis revealed that both subsets, $T_{fh}1$ and $T_{fh}17$, produced IL-2 and TNFα. However, IL-17 production was predominantly observed in IFNγ-negative, IL-21+ cells (**Supplementary Figure 5D**). To assess systemic levels of IL-21, we measured serum IL-21. We found a significant induction of IL-21 in both vaccine groups at day 7 post-immunization, with no observable differences observed across the adjuvant platforms (**Supplementary Figure 5E**). This suggests that the induction of IL-21 is a common feature of both vaccine formulations. Overall, these findings suggest that MPLA preferentially induces the production of IL-21+ IFNγ+ cells within the $T_{fh}1$ subset, while CAF01 promotes the generation of IL-21+ IL-17+ cells within

the $T_{fh}17$ subset. Furthermore, the $T_{fh}1/17$ subset exhibits the most diverse cytokine production profile among the subsets examined.

Next we investigated whether the effects of MPLA versus CAF01 adjuvants were also evident in cTfh responses. We observed a significant increase in proliferating cTfh cells, with a predominant induction of cTfh1 cells, similar to the phenotype observed in the LN, when MPLA was used as the adjuvant (**Figure 4H**). In contrast, no evidence of a $T_{fh}17$ or $T_{fh}1/17$ bias in cTfh cells was observed with CAF01 (data not shown). To evaluate Env-specific T_{fh} cell abundance, we utilized the AIM assay (**Supplementary Figure 5F**). The analysis showed a higher relative induction of Env-specific T_{fh} responses with MPLA at P1w1 but not P2w1 (**Figure 4I**), which was further corroborated by ICS assays (**Figure 4J**). The frequencies of CXCR5+ cells co-producing IL-2 and IFNγ, as well as cells co-producing IL-21 and IFNγ, indicated that higher numbers of IFNγ+ Env-specific cTfh cells were induced with MPLA at P1w1 and P2w1 (**Figure 4K**). Therefore, formulation of gp140 with MPLA induced strong T_h1-polarized GC T_{fh} responses, characterized by a higher magnitude of IFNγ+ anti-Env T_{fh} cells.

Induction of persistent anti-Env IgG antibodies with HIV-1 Env/MPLA+QS-21.

We next sought to determine whether induction of higher frequencies of Env-specific $T_{fh}1$ cells with MPLA could effectively enhance B cell proliferation and differentiation, in turn, promoting the development of Env antibodies with heightened affinity and increased durability. To this end, we performed a wide repertoire of quantitative and functional assays to assess the magnitude, durability, affinity, avidity, reactivity to Group M consensus protein, and effector functionality of vaccine induced humoral responses to Env. Longitudinal measures of binding antibody concentrations in sera against C.1086 Env showed rapid and equivalent recall in all animal's post P1, with antibodies reaching peak levels after the 2nd protein boost. While antibody kinetics were comparable across vaccine groups, significantly higher antibody magnitude was elicited by

MPLA at week 8 post 2nd boost and until 30 weeks after final immunization (**Figure 5A**). At this protracted memory time point, serum antibody concentrations were, on average, 2.5-fold higher with MPLA (median [ng/ml]; MPLA, 5566 versus CAF01, 2155) (**Figure 5B**). To assess CD4 correlates of antibody durability, we asked whether the magnitude of vaccine-elicited GC T_{fh} subsets after each boost predicted antibody concentrations at week 30. Frequencies of GC T_{fh} cells (at P1w2) were positively associated with antibodies at week 30 ($r = 0.6$, $p < 0.05$, data not shown). Two additional key cellular determinants of antibody durability emerged from our analysis: GC $T_{fh}1$ cell magnitude ($p < 0.05$, $r=0.65$) (**Figure 5C**) and frequencies of IFNγ+ IL-2+ Env-specific LN T_{fh} cells ($p < 0.05$, $r = 0.62$) (**Figure 5D**). These data in concert with IFNγ-regulated molecular programs induced in LN CD4 T cells support a role for GC $T_{fh}1$ induction in antibody persistence.

Using a binding antibody multiplex assay (BAMA), we further confirmed that stronger memory responses were elicited by MPLA, evidenced by higher median serum IgG antibody concentrations to C.1086 gp140 and gp120 antigens measured as area-under-the curve (AUC) over time (**Figure 5E-F**). Thus, utilizing two orthogonal approaches, the data showed significantly higher and protracted serum antibody responses against autologous Env with MPLA, indicative of efficient T_{fh} cell mediated B cell recruitment into the long-lived plasma cell pool.

We next sought to understand if induction of a $T_{fh}1$ profile was also associated with improved Env reactivity to Group M consensus proteins. Therefore, we tested serum reactivity against an antigen panel comprising of consensus gp140 proteins and found that antibodies with higher cross-clade reactivity were induced with MPLA relative to CAF01 (**Figure 5G-H**). We extended these analyses to assess reactivity to V1V2 loops of 1086C and noted that antibodies with

significantly higher specificity to these important regions within Env were induced in both vaccine regimens (**Figure 5I**).

Having established induction of robust serum Env antibodies with MPLA, we next determined whether Env-specific IgG reactivity would also be higher within rectal secretions. After normalization for total IgG levels within rectal secretions, the data showed that Env antibodies were effectively recalled in most animals at week 2 post 2nd protein boost and persisted in all animals 8 weeks after final immunization. However, akin to the systemic compartment, gp140 IgG in rectal secretions were significantly higher with MPLA at memory time point (**Figure 5J**), with 6-fold higher levels in MPLA relative to CAF01 at week 8 after final immunization (**Figure 5K**). In both vaccine regimens, the induction of Env-IgA antibodies was poor, preventing a quantitative assessment of IgA responses in secretions.

Induction of IgG1 subclass antibodies with greater effector functions with HIV-1 Env/MPLA+QS-21.

Since antibody effector functions, facilitated by interaction of Ig constant region with cognate Fc receptors on innate cells, mediate protection from acquisition and viral control (Carpenter and Ackerman 2020), we assessed the IgG subclass profile at week 2 post 2nd protein boost. Both CAF01 and MPLA+QS-21 induced Env-specific IgG1, and modest levels of IgG2, and IgG4 isotypes with higher IgG1 in all animals, with exception of one animal with higher IgG4 (**S6**).

Significantly higher IgG1 was induced by MPLA relative to CAF01 (**Figure 6A**), while IgG2 and IgG4 antibody subclasses were comparably induced (**Figure 6B-C**). The improved IgG1 subtype antibody responses with MPLA prompted us to determine whether a corresponding increase in antibody effector functions might also be observed. Measurement of antibody-

dependent phagocytosis (ADP) suggested enhanced effector functions with MPLA (**Figure 6D-E**) which strongly correlated with Env IgG1 but not IgG2 or IgG4 (**Figure 6F**).

Finally, we observed higher levels of neutralizing antibodies against the tier 1A MW965.26 at peak (2 weeks post 2nd protein boost) with MPLA relative to the CAF01 platform (**Figure 6G**). Antibody avidity measurements revealed relatively higher avidity with MPLA against autologous Env and to consensus Env proteins but not V1V2 loops (**Figure 6H-L**). Collectively, these findings provide evidence for significantly improved antibody quality associated with induction of GC $T_{fh}1$ cells.

Differentiation of GC T_{fh} Subsets initiated during the DNA Priming Phase.

Finally, we sought to determine the degree to which T_{fh} responses elicited during the priming phase influenced antibody responses post 1st protein boost. To this end, we analyzed blood samples at weeks 0, 1, 2, and 4, while also evaluating FNA of the draining LN at week 2 after the 3rd DNA prime (**Figure 7A**).

Animals were immunized with C.1086 DNA expressing IP10 (DNA_{IP10}) which primes stronger GC T_{fh} responses relative to DNA-alone (Verma, Schmidt et al. 2019). To further enhance GC T_{fh} responses, beyond that induced by DNA_{IP10}, we engineered DNA_{IP10} to co-express IL-6, a key cytokine promoting T_{fh} differentiation. Our vector achieved coordinate expression of Gag and Env antigens together with IP10+IL6 as confirmed in transfected 293T cells (**Figure 7B**). Following three rounds of intradermal immunization with DNA_{IP10} or $DNA_{IP10+IL6}$, we assessed proliferating cTfh cells (Ki-67^{+} PD-1^{+} of CXCR5+ CD4 T cells in blood, **Figure 7C**). We observed a significant increase at weeks 1 and 2 with $DNA_{IP10+IL6}$ but not DNA_{IP10} indicating that IP10+IL6 incorporation promoted T_{fh} differentiation. Additionally, T_{fh} induction was accompanied by notable $T_{fh}1$ skewing within proliferating cTfh cells (median cTfh1 at day 0 (% CD95), 0.89% versus 1.48% at day 7 and 14). Measurement of antigen-specific responses by AIM assay

demonstrated induction of Env and Gag-specific cTfh cells with a trend for higher responses elicited by $DNA_{IP10+IL6}$ (median, 0.42%, IQR 0.3- 1.7%) relative to D_{IP10} (median, 0.12%; IQR: 0.04 – 1.4%, **Supplementary Figure 7**).

Based on the transient accumulation of cTfh cells in the blood, we further explored GC T_{fh} responses. Out of twelve collected FNAs, eight were successful (four per vaccine group), and demonstrated significant increase in GC T_{fh} frequencies following vaccination (**Figure 7D**). Gating on Ki-67+ cells encompassing both CXCR5+ PD-1+ and PD-1++ subsets, an increase in activated T_{fh} cells within the LN was observed (**Figure 7E**), accompanied by a corresponding increase in the $T_{fh}1$ subset (**Figure 7F**). Altogether, these data demonstrate induction of GC $T_{fh}1$ responses during the priming phase post immunization with DNA_{IP10} or $DNA_{IP10+IL6}$.

Measurement of C.1086 Env antibodies in serum revealed induction of antibody responses after the 3rd prime in 8/12 animals, with comparable kinetics across vaccine groups. Notably, antibody concentrations 4 weeks post 3rd DNA prime strongly correlated with both the frequencies of proliferating T_{fh} cells (Ki-67+ PD-1+ CXCR5+) within the LN and with the proliferating $T_{fh}1$ (Ki-67+ PD-1+ CXCR5+ CXCR3+) subset at 2 weeks post 3rd DNA prime (**Figure 7G-H)**. Moreover, the strong association of antibody concentrations after the 3rd DNA prime with peak antibodies following the 1st protein boost (**Figure 7I**) indicated efficient recall of Env-specific memory B cells induced during the prime. Overall, the data show that stimulation of $T_{fh}1$ cells during the DNA priming stage is closely linked with robust antibodies post boost.

In summary, our results strongly support maximizing GC $T_{fh}1$ responses during both the prime and boost phases as a strategy to generate potent and durable humoral immunity. These findings have significant implications for the development of more effective vaccination strategies aimed at eliciting robust and long-lasting immune responses.

DISCUSSION

T_{fh} cells are fundamental in establishing long-lasting humoral immunity with vaccination. The dynamic interplay between innate immune activation and the ensuing inflammatory response directs the magnitude and composition of T_{fh} cell populations, ultimately shaping quantitative and qualitative features of humoral memory (Hirota, Turner et al. 2013, Barbet, Sander et al. 2018, Olatunde, Hale et al. 2021). Here we show that maximizing induction of CXCR3+ $T_{fh}1$ cells correlates with serum Env antibodies which exhibit higher persistence. Our studies with LAMV revealed the robust induction of cTfh1 and GC $T_{fh}1$ responses, along with a moderate induction of $T_{fh}17$ and $T_{fh}1/17$ cells. These findings led us to compare the adjuvants MPLA+QS-21 and CAF01, known to elicit T_h1 and mixed $T_h1/17$ responses (Christensen, Bollehuus Hansen et al. 2019), (Pedersen, Andersen et al. 2018) respectively, to determine the optimal strategy for maximizing Env antibody persistence. Through proteomic and transcriptomic analysis of lymph nodes, we uncovered evidence of robust GC responses induced by both vaccine adjuvants following a DNA prime. Moreover, we observed notable skewing of T_{fh} responses, which corresponded with the elicitation of distinct immunogenicity profiles. Interesting, although peak antibody responses following each protein boost were similar across the vaccine platforms, our investigation revealed a notable distinction in antibody persistence. Specifically, the MPLA+QS-21 regimen exhibited higher antibody levels at week 8,12, and 30, suggestive of enhanced support from T_{fh} cells in promoting plasma cell differentiation.

Moreover, $T_{fh}1$ cell induction during the DNA priming phase was linked to effective boosting upon subsequent protein immunization. These findings highlight the critical role of $T_{fh}1$ cells in driving the longevity of antibody responses and emphasize the potential of stimulating $T_{fh}1$ cells during the prime and boost to elicit durable humoral immunity against HIV Env.

A significant finding in RV144 vaccine recipients was the correlation between Env-specific circulating CD4 T cell subsets co-producing IFNγ, TNFα, CD40L, and IL4, and a reduced risk of HIV acquisition [40]. This correlation suggests that productive GC responses elicited by the vaccine fostered protective humoral immunity (Lin, Finak et al. 2015). More recently, follow up analysis of this population in n=6 subjects immunized with the RV144 vaccine regimen in South Africa (HVTN 097) reported a pT_h2 biased transcriptional profile based on observed IL4 and IL13 transcripts (Cohen, Tian et al. 2022). However, it is important to note that in addition to T_h2 cells, CD4 T_{fh} cells also produce IL-4 in a SLAM/SAP dependent manner (McCausland, Yusuf et al. 2007) and T_h1 cells can produce IL-13 in the presence of IL18 (Hayashi, Yoshimoto et al. 2007). These findings indicate the need for utilizing multiple immune parameters when categorizing CD4 T cell help and underscore the importance of studying both lymph node and peripheral blood CD4 T_{fh} cells to fully understand their respective roles in fostering Env antibody responses.

In the context of vaccination, our observed association between $T_{fh}1$ cells and persistent antibody responses raises the possibly that higher relative production of IL-21 and CD40L may support the proliferation of GC B cells in concert with IFNγ-mediated B cell proliferation. This contention is supported by the observation of higher relative Ki-67 protein levels in the MPLA group at week 2 of the first protein boost. In the context of a T_h1 driven GC response rich in CXCL chemokines CXCL9, 10, and 11; CXCR3 expression on T_{fh} cells may furthermore enable proximity and interaction with GC B cells. CAF01 is composed of cationic liposomal vesicle

(dimethyldioctadecylammonium, DDA) together with a synthetic analog of a mycobacterial cell wall (trehalose dibehenate, TDB), a potent activator of macrophages and dendritic cells through the macrophage inducible $Ca2^{+}$-dependent lectin receptor Mincle, a pattern recognition receptor recognizing bacterial lipids (Davidsen, Rosenkrands et al. 2005, Martinez-Lopez, Iborra et al. 2019). CAF01 elicits CD4 T_h1 responses while concurrently driving strong T_h17 responses to a mycobacterium TB subunit vaccine via induction of proinflammatory cytokines IL-1β, IL-6, and TNF-α (Werninghaus, Babiak et al. 2009). We observed that CAF01 was effective in inducing robust cellular responses, which were skewed towards a T_h1/T_h17 profile within GCs. It is possible that employing the CAF06 platform which incorporates MPL into the bilayer of DDA/TDB liposomes may drive stronger T_h1 responses together with T_h17 cells thereby enhancing protective immunity by eliciting strong humoral immune responses.

The present studies are the first to our knowledge to assess immunological responses across HIV vaccine platforms with MPLA and CAF01-based adjuvants and strongly support GC $T_{fh}1$ cell induction for enhancing Env antibody responses. However, our study has several limitations. First, priming modalities across MPLA and CAF01 were not identical. Animals boosted with MPLA were primed with DNA_{IP10}, whereas CAF01 boosted animals received the $DNA_{IP10+IL6}$ prime. Given the stronger immunogenicity of $DNA_{IP10+IL6}$, it is possible that our studies underestimate immune recall potential of MPLA relative to CAF01. Second, 5/6 animals in each vaccine group were males and therefore our findings do not capture possible variability in vaccine response between sexes. Because females develop higher antibody responses than males, it is important to test our hypothesis in animals of both sexes (Fischinger, Boudreau et al. 2019). Third, the interplay of innate immune cells and the follicular dendritic cell network in regulation of T_{fh} help for antibody responses is an important consideration for future studies. In this context, conducting mechanistic studies involving cytokine blockade to assess its impact on T_{fh} differentiation in vivo is essential for establishing the significance of adjuvants in shaping

humoral immunity. Finally, we did not assess vaccine efficacy and therefore whether GC $T_{fh}1$ cells constitute an important correlate of protection from acquisition remains an important unanswered question.

In summary, our findings demonstrate significant skewing of the GC T_{fh} response by adjuvants inducing distinct inflammatory responses. We further demonstrate that induction of $T_{fh}1$ cells results in superior persistence of Env antibodies indicating that strategies to harness this CD4 subset may promote protective humoral immunity against HIV.

MATERIALS AND METHODS

Table 1: Flow Cytometry Antibodies

Antibody name	Panel	Vendor	Catalog number/Identifier
Mouse anti-human CD3 (Clone SP34-2)	T_{FH}/AIM/ICS	BD Biosciences	Cat#557917; RRID: AB_396938
Mouse anti-human CD4 (Clone L200)	T_{FH}/AIM/ICS	BD Biosciences	Cat#563737; RRID: AB2687486
Mouse anti-human CD8 (Clone SK-1)	T_{FH}/AIM/ICS	BD Biosciences	Cat#564913; RRID: AB_2833078
Mouse anti-human CD14 (Clone MSE2)	T_{FH} Panel	BioLegend	Cat#301822; RRID: AB_493747
Mouse anti-human CD16 (Clone 3G8)	T_{FH} Panel	BD Biosciences	Cat#563172; RRID: AB_2744297
Mouse anti-human CD20 (Clone 2H7)	T_{FH} Panel	BioLegend	Cat#302314; RRID: AB_314262
Mouse anti-human CD69 (Clone FN50)	T_{FH} Panel	BioLegend	Cat#310944; RRID: AB_2566466
Mouse anti-human CD95 (Clone DX2)	T_{FH}/AIM/ICS	BioLegend	Cat#564710; RRID: AB_2738907
Mouse anti-human CXCR3 (CD183) (Clone 1C6)	T_{FH} Panel	BD Biosciences	Cat# 550967; RRID: AB_398481
Mouse anti-human CXCR5 (CD185) (Clone MU5UBEE)	T_{FH}/AIM/ICS	eBioscience	Cat#12-9185-42; RRID: AB_11219877
Mouse anti-human CCR6 (CD196) (Clone G034E3)	T_{FH} Panel	BioLegend	Cat#353430; RRID: AB_2564233
Armenian Hamster anti- ICOS (CD278) (Clone C396.4A)	T_{FH} Panel	BioLegend	Cat#313534; RRID: AB_2629729
PECy7 anti-human PD1 (CD279) (Clone EH12.2H8)	T_{FH} Panel	BioLegend	Cat# 329918, RRID: AB_2159324
Mouse anti-human Bcl-6 (Clone	T_{FH} Panel	BD	Cat# 563581

K112-91)		Biosciences	
Mouse anti-Ki-67 (Clone B56)	T_{FH} Panel	BD Biosciences	Cat#558616; RRID: AB_10611866
Mouse anti-human CD25 (Clone BC96)	AIM assay	eBioscience	Cat#**53-0259-42** RRID: AB_2043827
Mouse anti-human CD134 (OX-40) (Clone L106)	AIM assay	BD Biosciences	Cat#744746; RRID: AB_2742454
Mouse anti-human CD137 (4-1BB) (Clone 4B4-1)	AIM assay	BioLegend	Cat# 309826; RRID: AB_2566260
Mouse anti-human CD154 (CD40L) (Clone 24-31)	AIM assay	eBioscience	Cat#17154842 RRID:AB_1582215
Mouse anti-human TNF-α (Clone Mab11)	ICS assay	BioLegend	Cat# 502906; RRID: AB_315258
Mouse anti-human IFNγ (Clone B27)	ICS assay	BioLegend	Cat# 506518; RRID: AB_2123321
Mouse anti-human IL2 (Clone MO1-17H12)	ICS assay	BioLegend	Cat# 500344; RRID: AB_2564091
Mouse anti-human IL-17 (Clone eBio64DEC17)	ICS assay	eBioscience	Cat# 48-7179-42; RRID: AB_10853643
Mouse anti-human IL-21 (Clone 3A3-N2.1)	ICS assay	BD Biosciences	Cat# 560493; RRID: AB_1645421
APC-Cy7 live/dead		Life Technologies	Cat#L34976
BV510 live/dead		Life Technologies	Cat#L34966

Table 2. Samples for RNA seq and Spatial profiling

S.No	**Animals ID**	**Vaccine group**	**Lymph node collection time points and cells used for**		
			Baseline (WK0)	**Week2 post 1st protein boost**	**Week3 post 2nd protein boost**
1	**47161**	MPLA+QS-21	RNA seq	RNA seq	RNA seq
2	**45781**	MPLA+QS-21	Spatial profiling	Spatial profiling	Spatial profiling
3	**46235**	MPLA+QS-21	Spatial profiling	Spatial profiling	Spatial profiling
4	**46551**	MPLA+QS-21	Spatial profiling	Spatial profiling	Spatial profiling
5	**46548**	MPLA+QS-21	RNA seq	RNA seq	RNA seq
6	**47081**	MPLA+QS-21	RNA seq	RNA seq	RNA seq
7	**45721**	CAF01	RNA seq+Spatial profiling	RNA seq+Spatial profiling	RNA seq+Spatial profiling
8	**47154**	CAF01	NA	NA	NA
9	**46410**	CAF01	Spatial profiling	Spatial profiling	Spatial profiling
10	**46354**	CAF01	RNA seq	RNA seq	RNA seq
11	**47466**	CAF01	RNA seq	RNA seq	RNA seq
12	**47387**	CAF01	Spatial profiling	Spatial profiling	Spatial profiling

Rhesus Macaques. For LAMV studies, sixteen female colony-bred Indian origin rhesus macaques (*Macaca mulatta*) were utilized. Animals were dichotomized by age into two groups; young [n=8, mean=4 years] and aged [n=8, mean=16 years]. Young adults with a higher baseline weight [mean=5.9kg] were selected for the cohort to closer match the aged animals in size [mean=8.6kg]. For the HIV vaccine study, twelve adult (10 males and 2 females) Indian origin rhesus macaques (*Macaca mulatta*) were utilized. At study initiation, animals were 3.4 – 5.6 years of age with a median weight of 6.8 kg. Animals in both studies were SIV negative (SIV-), simian T-cell leukemia virus negative (STLV-), and simian retrovirus negative (SRV-); and had no history of dietary, pharmacological, or surgical manipulation (*Supplementary Table 1a*). All animals were bred and housed at the California National Primate Research Center (CNPRC) in accordance with the American Association for Accreditation of Laboratory Animal Care (AAALAC) guidelines. All studies were approved by the University of California, Davis Institutional Animal Care and Use Committee (IACUC).

LAMV Immunization. The animals received an IM booster vaccination of canine distemper-measles vaccine (Vanguard).

HIV-1 Immunization. Animals were immunized with DNA vaccines intradermally in both thighs at weeks 0, 4, and 8. At each prime, animals received 4mg of the pGA2/JS2 plasmid DNA encoding either SHIV C.1086 T/F Env + rhesus interferon-induced protein (IP)-10 (Group 1; n=6) or SHIV C.1086 T/F Env + rhesus interferon-induced protein (IP)-10 + rhesus interleukin (IL)-6 (Group 2; n=6). Subsequent protein boosters were administered at weeks 12 and 20 with Group 1 animals receiving 50µg C.ZA 1197MB gp140 protein adjuvanted with MPLA + QS-21 and Group 2 animals receiving 50µg C.ZA 1197MB gp140 protein adjuvanted with CAF01 delivered in a 175µL volume subcutaneously into each thigh.

Cationic Adjuvant Formulation 01 (CAF01). CAF01 was generously provided by Statens Serum Institut, Denmark. Admixing with protein was performed by addition of 25µg of C.ZA 1197MB gp140 protein (Immune Technology, USA) to 250µL of CAF01 (625µg DDA+ 125µg TDB) adjuvant formulation. The solution was vortexed vigorously for 15-30 seconds followed by visual inspection. Remaining protein was added in 10µg increments with intermittent vortexing until a final amount of 100µg gp140 was achieved.

Monophosphoryl Lipid A (MPLA). Synthetic MPLA was purchased from InvivoGen, USA. 100µg C.ZA 1197MB gp140 protein was dissolved in a solution of 100µg MPLA with 50µg QS-21 saponin [Desert King International, USA] (2:2:1) in PBS.

Specimen collection and processing. Lymph node (LN) biopsies were obtained at baseline (week0), week 14 (week 2 post 1st protein boost) and week 23 (week 3 post 2nd protein boost) and processed as described previously (Verma, Schmidt et al. 2019). Isolated cells were washed in complete media, counted, and cryopreserved until subsequent analysis. Two weeks after the 3rd DNA immunization, fine needle aspirates of LN were obtained using a 22-gauge needle, as previously described (Verma, Schmidt et al. 2019). PBMCs were isolated from whole blood collected in CPT vacutainer tubes at weeks 0, 4, 9, 10, 13, 21, and 32 . Serum was collected from animals at weeks 0, 4, 8, 8+day3, 9,10, 12, 13, 14, 16, 20, 20+day3, 21, 22, 23, 28, 32, 50 timepoints and stored at -80°C until subsequent analysis. Rectal secretions were collected for assessment of mucosal antibody production using premoistened Weck-Cel sponges as previously described (Verma, Schmidt et al. 2019).

Activation induced Marker and Intracellular cytokine staining assay. Detection of antigen specific CD4 T cells detection was quantified by activation induced marker (AIM) and intracellular cytokine staining (ICS). PBMCs/LN cells were stimulated with overlapping peptide pools of HIV consensus C and HIV-1 C.1086 Env gp140C protein (NIH AIDS Reagent Program) in AIM/R10 media in the presence of 0.2µg CD28/49d co-stimulatory antibodies (BD) per test. As a positive control, cells were stimulated with 1X Cell Stimulation Cocktail (PMA and ionomycin) (eBioscience, USA). Unstimulated controls were treated with volume-controlled DMSO (Sigma-Aldrich). Tubes were incubated in 5% CO_2 at 37°C overnight for AIM assay. For ICS assay, after 1 hour of stimulations, protein transport inhibitors 2µl/mL GolgiPlug (Brefeldin A) and 1.3µl/mL GolgiStop (Monensin) (BD, Biosciences, USA) were added to the tubes for 8 hours at 37°C, 5% CO_2. Following stimulation, the cells were stained for AIM and ICS surface markers (see **Table 1**). Cells were then fixed with cytofix/cytoperm for 10 min at 4°C, permeabilized with 1X Perm wash buffer (BD, Biosciences, USA), and stained for intracellular markers (see **Table 1**) for 45 min. Cells were then washed and acquired the same day on a BD FACS Symphony.

T_{fh} cell staining by flow cytometry and cell sorting. T_{fh} cell staining was performed on whole blood and LN cells as previously described (Verma, Schmidt et al. 2019). Samples were acquired on BD FACS Symphony with FACS Diva version 8.0.1 software and data were analyzed using FlowJo (Versions 9 and 10). For cell sorting, cryopreserved cells were enriched by NHP CD4 isolation kit (Miltenyi Biotec,USA) and stained with CD3, CD4, CXCR5, CD95, and live/dead in complete media (incubated for 1 hour at 4°C on a shaker). Stained cells were washed twice with 5mL RPMI plain media (Gibco, USA) and resuspended in 0.5mL of sorting buffer containing 2% FBS+PBS. The cells were then filtered through a 40µM strainer into 5mL sterile FACS tube (Blue cap tube). Cell sorting was performed using a BD FACSAria III. Naive,

and CD95+ CD4 T cell populations were collected in complete media supplemented with 20% FBS. Sorted cells were stimulated with overlapping peptide pools of HIV consensus C and HIV-1 C.1086 Env gp140C protein (NIH AIDS Reagent Program) in R10 media in the presence of 0.2µg/mL CD28/49d co-stimulatory antibodies (BD) for 14 hours. The culture supernatant and stimulated cells were collected and stored at -80°C for subsequent analysis.

Serum IL-21 ELISA. Serum IL-21 cytokine was quantified using an IL-21 ELISA Development kit (Novus Bio, USA) in accordance with manufacturer's protocol. Briefly, the capture mAb (MT216G) was diluted to 2µg/mL in PBS, pH 7.4 and added (100µL/well) to 96-well microtiter plates with high binding capacity (Thermo Fisher, USA) and incubated overnight at 4°C. The next day, plates were aspirated, and wells blocked with 200µL/well of PBS with 0.05% Tween 20 and 0.1% BSA (incubation buffer). After 1 hour of incubation, plates were washed 5 times with PBS containing 0.05% Tween 20 (300µL/well). Samples or working standards were added at 100uL/well and incubated for 2 hours at room temperature. After washing, plates were incubated for one hour with 100µL/well of detection mAb diluted to 1µg/mL in incubation buffer. Streptavidin-HRP conjugates were diluted 1: 1000 in incubation buffer and added to the plates at 100uL/well for 1 hour followed by washing. Plates were washed and then developed with TMB substrate (Thermo Fisher, USA), and the reaction quenched with 0.2M H_2SO_4 (Sigma, USA). Absorbance was recorded using a Spectramax 5 plate reader (Molecular Devices) at 450 nm with a reference filter at 570 nm within 15 min. The concentration of IL-21 in serum was calculated based on an IL-21 standard curve using SoftMax Pro.

RNA Sequencing and Bioinformatics. RNA was extracted from sorted naive, and CD95+ CD4 T cells using a RNeasy plus mini kit (QIAgen). Isolated RNA sample quality was assessed using a BioAnalyzer RNA pico assay (Agilent Technologies Inc., California, USA) and quantified by Qubit 2.0 RNA HS assay (ThermoFisher, Massachusetts, USA). Library construction was

performed based on manufacturer's recommendation for the SMART-Seq® v4 Ultra® Low Input RNA Kit (Takara Bio USA Inc., California, USA) followed by the Nextera® XT DNA Library Prep Kit (Illumina, California, USA). Final library quantity was measured using the KAPA SYBR® FAST qPCR and library quality evaluated using a TapeStation D1000 ScreenTape (Agilent Technologies, CA, USA). Final library size was about 450bp with an insert size of about 300bp. Illumina® 8-nt dual-indices were used. Equimolar pooling of libraries was performed based on QC values and sequenced on an Illumina® NovaSeq S4 (Illumina, California, USA) with a read length configuration of 150 PE for 40 M PE reads per sample (20M in each direction). Reference rhesus macaque genome (*Macaca_mulatta* _GCF_003339765.1_Mmul_10) and gene model annotation files were downloaded directly from the genome website. Index of the reference genome was built using Hisat2 v2.0.5 and paired-end clean reads were aligned to the reference genome using Hisat2 v2.0.5. The mapped reads of each sample were assembled by StringTie (v1.3.3b) using a reference-based approach.

The quality of the raw RNA-seq data was assessed using FastQC and poor-quality ends were trimmed (Trimgalore). High-quality sequences were aligned against the Macaca mulatta reference genome using STAR aligner v2.7.9, and counts were generated using featureCount (Dobin, Davis et al. 2013). A list of differentially expressed genes (DEGs) were generated using DESeq2 based on the negative binomial distribution(Love, Huber et al. 2014). The resulting DEGs between the groups were defined at cut-off criteria of $|\log_2 \text{fold-change}| \geq 1.5$ and *p*-value < 0.05 adjusted using the Benjamini and Hochberg's approach for controlling the false discovery rate (Liao, Smyth et al. 2013). Gene set enrichment analysis (Subramanian, Tamayo et al. 2005) was used to assess the statistical enrichment of gene ontologies and pathways, and visualized using Clusterprofiler v4.8.1(2012). All statistical analyses were performed using R 4.2.0.

GeoMx Digital Spatial Profiling (DSP). Formalin-fixed paraffin-embedded (FFPE) blocks were prepared using lymph node tissue from biopsies at baseline, week 2 post protein1, and week 3 post protein 2 immunization timepoints to analyze the spatial protein profiling using the Nanostring GeoMx Digital Spatial Profiler (DSP). Tissue sections of 5-µm thickness were cut from FFPE blocks and mounted on GeoMx-NGS BOND RX slide as per manufacturer's recommendations. Sections were baked at 60°C for 30 minutes, deparaffinized, rehydrated in CitriSolv, ethanol and washed in water. For antigen retrieval, slides were placed in a staining jar containing 1X Citrate Buffer (pH 6) for 15 minutes using a preheated pressure cooker (high pressure and high temp). The tissue slides were washed with 1X TBS-T and blocked with Buffer W for 1 hour at room temperature in a closed humidity chamber. Tissue slides were stained with a cocktail of fluorescent morphological markers SYTO13 (nuclear stain; AF532), CD20 (Clone: L26; AF488), CD3 (Clone: CD3-12; AF594), and Ki-67 (Clone: B56; AF647) at 1:10000, 1:250, 1:100, and 1:1000 dilutions, respectively. For protein detection, a multiplex cocktail of primary antibodies was used from core panels; GeoMx immune cell profiling panel, GeoMx IO drug target module, and GeoMx immune activation status module (*See* ***supplementary Table2***). In total, 60 regions of interest (ROIs) were selected within GCs based on co-localization of CD3 with CD20+ Ki-67+ GC B cells. Indexing oligos were released from each ROI by exposure to UV light as described(Merritt, Ong et al. 2020), and 10µl of liquid from above the ROI was collected by a microcapillary tip and deposited in a 96-well plate.

Indexing oligos from each ROI were PCR amplified using GeoMx Seq Code primers. PCR products were pooled and purified twice with AMPure XP beads (Beckman Coulter, Brea, CA). Library concentration and purity were measured using a high-sensitivity DNA Bioanalyzer chip (Agilent Technologies, Santa Clara, CA). Paired-end sequencing was performed on an Illumina HiSeq 2000 instrument (Illumina, San Diego, CA). After sequencing, fastq files were run through the GeoMx NGS Pipeline where reads were trimmed, merged, and aligned to a list of indexing oligos to identify the source probe. Analysis of filtered normalized gene expression data was

performed in R with Bioconductor. We profiled 32 proteins along with core protein in GeoMx Human Protein array. We first calculated the signal-to-noise ratio by dividing raw count values by the geometric mean of the negative IgG probes. The data were normalized using three negative control IgG probes with the GeomxTools package. Normalized expression values were used for downstream analyses. Dimensionality reduction analysis was performed with principal component analysis using the facomineR package(Lê, Josse et al. 2008). Differential expression analysis was conducted with the mixedModelDE function from the GeomxTools package. We tested for differences between time points and/or vaccine groups using linear mixed effect models that incorporated animal ID as a random effect term to account for non-independence of the multiple ROIs sampled per animal. Differential expression results were visualized in heatmap plots generated using the ComplexHeatmap R package(Gu, Eils et al. 2016).

Serum IgG ELISA. Serum IgG titers against HIV-1 C.1086 Env gp140 were determined by ELISA as described previously (Verma, Schmidt et al. 2019). In brief, 96-well microtiter plates with high binding capacity (Thermo Fisher, USA) were coated overnight at 4°C with C.1086 Env gp140 protein from the NIH AIDS Reagent Program (ARP) diluted in coating buffer. Plates were washed and blocked with nonfat dry milk in PBS for two hours at room temperature and washed five times with 1X PBS-0.05% tween-20 (PBST). Diluted standard and serum samples were added to plate wells and incubated overnight at 4°C. Plates were washed, and HRP conjugated goat anti-monkey IgG (Nordic MUbio, Netherlands) was added to plate wells and incubated at room temperature for 1 hour. Plates were then washed and developed with the addition of TMB substrate (Thermo Fisher, USA). Absorbance was recorded at 450 nm with a reference filter at 570 nm using a Spectramax 5 plate reader (Molecular Devices, USA). Baseline sera from each animal served as negative control and optical density (OD) values 2-fold above baseline were

considered positive and extrapolated using in-plate standards to determine anti-Env antibody concentrations.

IgG subclass antibodies. ELISA was used to measure concentrations of gp120-specific IgG1-4 antibodies. Ten rows of a 96-well Immulon 4 microtiter plate (VWR) were coated overnight at 4˚C with 50ng C.1086 gp120Δ7 (HIV Reagent Program) per well in PBS, pH 7.2. To generate a standard curve with a known amount of IgG1, IgG2, IgG3 or IgG4 antibody, 2 rows of the plate were coated with 50ng per well recombinant CD40 (NHP Reagent Resource). The following day, the plate was washed with PBST and blocked with PBST containing 0.1% BSA (ELISA buffer: EB). Serum samples diluted in EB were then added to gp120 wells. Duplicate dilutions of anti-CD40 rhesus IgG1, IgG2, IgG3 or IgG4 antibody (NHP Reagent Resource) were added to the CD40 wells. Following overnight incubation at 4˚C, the plate was washed and treated for 1h at 37˚C with 0.5µg/ml of the appropriate biotinylated monoclonal antibody (all from NHP Reagent Resource) diluted in EB: anti-rhesus IgG1 clone 7H11 (ena), anti-rhesus IgG2 clone 8D11 (dio), anti-rhesus IgG3 clone 6F5 (tria) or anti-rhesus IgG4 clone 7A8 (tessera). Plates were washed, treated with 1/4,000 diluted neutralite avidin peroxidase (SouthernBiotech) for 30min at room temperature, developed with TMB substrate and quenched with a H_2SO_4 stop solution. After recording absorbance at 450nm, a standard curve constructed from the anti-CD40 IgG subclass antibody was used to interpolate the concentration of anti-gp120 IgG of the same subclass in samples

ADP assay. Serum antibodies were evaluated for ability to enhance phagocytosis of gp120 expressing fluorescent beads by THP-1 monocytes as previously described (Verma 2020). Briefly, 1µm avidin-coated fluorospheres (Invitrogen) were labeled with biotinylated anti-His tag monoclonal antibody (ThermoScientific) and used to capture His-tagged clade C gp120 Du151 protein (Immune Technologies). The gp120-expressing beads were then incubated with

triplicate 5-fold dilutions of heat-inactivated serum samples in V-bottom plates for 1h at 37˚C. THP-1 cells ($2x10^4$ per well) were then added and incubated at 37°C in 5% CO_2. After 5h, cells were washed with $Ca^{+2/}Mg^{+2}$-free DPBS, then treated with 0.12% trypsin-EDTA for 5 min at 37°C. The cells were washed and resuspended in 1% paraformaldehyde. Fluorescence was measured using a FACSCanto (BD Biosciences) and FlowJo 9 software. Phagocytosis was quantified by multiplying the percentage of fluorescent cells by their median fluorescence intensity. A phagocytic score was then calculated by dividing the phagocytosis measured in each test sample by the phagocytosis observed for pooled pre-immune serum at the same dilution.

Neutralization assay. Serum neutralizing activity was quantified using a previously described pseudovirus infectivity assay where TZM-bl cells were co-incubated with tier 1 clade C pseudovirus MW965.26, tier 2 clade C virus Ce1086_B2, tier 2 clade C Ce1176_A3, or a control MLV-pseudotyped virus (to measure non-HIV-specific activity). Neutralization titers were measured in serum samples collected at week 0 and week 2 following the 2nd protein boost. Samples neutralizing antibody activity against SIV pseudoviruses was measured relative to MLV pseudovirus negative controls.

Mucosal antibodies. A custom binding antibody multiplex assay (BAMA) assay with C.1086 gp140 K160N-conjugated Bio-Rad Bio-plex Pro magnetic COOH beads was used to quantify Env-specific IgG in rectal secretions and specific IgA in IgG-depleted sera and rectal secretions as previously described (Verma, Schmidt et al. 2019). Briefly, 50µg gp140 was conjugated to 10 x 10^6 beads as described (Iyer, Gangadhara et al. 2015). The gp140-labeled beads (3500 per well) were shaken overnight at 1100 rpm and 4˚C with 10-fold dilutions of serum or secretion and standard [Verma 2020]. Beads were then washed with PBST and reacted for 30 minutes at room temperature with biotinylated goat anti-human IgG (Southern Biotech) or goat whole IgG

containing anti-monkey IgA (Novus) followed by phycoerythrin-labeled neutralite avidin (Southern Biotech). Fluorescence was measured with a Bio-Rad Bioplex 200. Antibody concentrations were determined using standard curves prepared with Bioplex Manager software (Bio-Rad). Concentrations of gp120-specific IgG in secretions were divided by the concentration of total IgG or IgA measured in the sample by ELISA to obtain the specific activity (ng of gp140-specific IgG or IgA antibody per µg of total IgG or IgA, respectively).

Statistical analysis. Statistical analysis was performed using Prism v.9.5.1 (Graph Pad). Gaussian distribution was not assumed, thus comparisons across time, between groups, and correlations were analyzed using non-parametric tests. For within group comparisons, Wilcoxon matched pairs signed rank test was used. For between group comparisons, Mann-Whitney rank comparisons were used. Correlation coefficients were computed using Spearman correlation. P values < 0.05 were considered significant.

REFERENCES

(2012). "clusterProfiler: an R Package for Comparing Biological Themes Among Gene Clusters." OMICS: A Journal of Integrative Biology **16**(5): 284-287.

Alving, C. R., K. K. Peachman, M. Rao and S. G. Reed (2012). "Adjuvants for human vaccines." Curr Opin Immunol **24**(3): 310-315.

Barbet, G., L. E. Sander, M. Geswell, I. Leonardi, A. Cerutti, I. Iliev and J. M. Blander (2018). "Sensing Microbial Viability through Bacterial RNA Augments T Follicular Helper Cell and Antibody Responses." Immunity **48**(3): 584-598 e585.

Carpenter, M. C. and M. E. Ackerman (2020). "Recent insights into Fc-mediated effector responses to HIV-1." Curr Opin HIV AIDS **15**(5): 282-289.

Christensen, D., L. Bollehuus Hansen, R. Leboux, W. Jiskoot, J. P. Christensen, P. Andersen and J. Dietrich (2019). "A Liposome-Based Adjuvant Containing Two Delivery Systems with the Ability to Induce Mucosal Immunoglobulin A Following a Parenteral Immunization." ACS Nano **13**(2): 1116-1126.

Cohen, K. W., Y. Tian, C. Thayer, A. Seese, R. Amezquita, M. J. McElrath, S. C. De Rosa and R. Gottardo (2022). "Th2-Biased Transcriptional Profile Predicts HIV Envelope-Specific Polyfunctional CD4(+) T Cells That Correlated with Reduced Risk of Infection in RV144 Trial." J Immunol **209**(3): 526-534.

Crotty, S. (2014). "T follicular helper cell differentiation, function, and roles in disease." Immunity **41**(4): 529-542.

Davidsen, J., I. Rosenkrands, D. Christensen, A. Vangala, D. Kirby, Y. Perrie, E. M. Agger and P. Andersen (2005). "Characterization of cationic liposomes based on dimethyldioctadecylammonium and synthetic cord factor from M. tuberculosis (trehalose 6,6'-

dibehenate)-a novel adjuvant inducing both strong CMI and antibody responses." Biochim Biophys Acta **1718**(1-2): 22-31.
Dobin, A., C. A. Davis, F. Schlesinger, J. Drenkow, C. Zaleski, S. Jha, P. Batut, M. Chaisson and T. R. Gingeras (2013). "STAR: ultrafast universal RNA-seq aligner." Bioinformatics **29**(1): 15-21.
Eisinger, R. W. and A. S. Fauci (2018). "Ending the HIV/AIDS Pandemic(1)." Emerg Infect Dis **24**(3): 413-416.
Fabregat, A., K. Sidiropoulos, G. Viteri, O. Forner, P. Marin-Garcia, V. Arnau, P. D'Eustachio, L. Stein and H. Hermjakob (2017). "Reactome pathway analysis: a high-performance in-memory approach." BMC Bioinformatics **18**(1): 142.
Fauci, A. S. (2017). "An HIV Vaccine Is Essential for Ending the HIV/AIDS Pandemic." JAMA **318**(16): 1535-1536.
Felber, B. K., Z. Lu, X. Hu, A. Valentin, M. Rosati, C. A. L. Remmel, J. A. Weiner, M. C. Carpenter, K. Faircloth, S. Stanfield-Oakley, W. B. Williams, X. Shen, G. D. Tomaras, C. C. LaBranche, D. Montefiori, H. V. Trinh, M. Rao, M. S. Alam, N. A. Vandergrift, K. O. Saunders, Y. Wang, W. Rountree, J. Das, G. Alter, S. G. Reed, P. P. Aye, F. Schiro, B. Pahar, J. P. Dufour, R. S. Veazey, P. A. Marx, D. J. Venzon, G. M. Shaw, G. Ferrari, M. E. Ackerman, B. F. Haynes and G. N. Pavlakis (2020). "Co-immunization of DNA and Protein in the Same Anatomical Sites Induces Superior Protective Immune Responses against SHIV Challenge." Cell Rep **31**(6): 107624.
Fischinger, S., C. M. Boudreau, A. L. Butler, H. Streeck and G. Alter (2019). "Sex differences in vaccine-induced humoral immunity." Semin Immunopathol **41**(2): 239-249.
Gao, X., K. Luo, D. Wang, Y. Wei, Y. Yao, J. Deng, Y. Yang, Q. Zeng, X. Dong, L. Xiong, D. Gong, L. Lin, K. Pohl, S. Liu, Y. Liu, L. Liu, T. H. O. Nguyen, L. F. Allen, K. Kedzierska, Y. Jin, M. R. Du, W. Chen, L. Lu, N. Shen, Z. Liu, I. A. Cockburn, W. Luo and D. Yu (2023). "T follicular helper 17 (Tfh17) cells are superior for immunological memory maintenance." Elife **12**.
Gu, Z., R. Eils and M. Schlesner (2016). "Complex heatmaps reveal patterns and correlations in multidimensional genomic data." Bioinformatics **32**(18): 2847-2849.
Hayashi, N., T. Yoshimoto, K. Izuhara, K. Matsui, T. Tanaka and K. Nakanishi (2007). "T helper 1 cells stimulated with ovalbumin and IL-18 induce airway hyperresponsiveness and lung fibrosis by IFN-gamma and IL-13 production." Proc Natl Acad Sci U S A **104**(37): 14765-14770.
Henriksen-Lacey, M., D. Christensen, V. W. Bramwell, T. Lindenstrom, E. M. Agger, P. Andersen and Y. Perrie (2011). "Comparison of the depot effect and immunogenicity of liposomes based on dimethyldioctadecylammonium (DDA), 3beta-[N-(N',N'-Dimethylaminoethane)carbomyl] cholesterol (DC-Chol), and 1,2-Dioleoyl-3-trimethylammonium propane (DOTAP): prolonged liposome retention mediates stronger Th1 responses." Mol Pharm **8**(1): 153-161.
Hill, D. L., W. Pierson, D. J. Bolland, C. Mkindi, E. J. Carr, J. Wang, S. Houard, S. W. Wingett, R. Audran, E. F. Wallin, S. A. Jongo, K. Kamaka, M. Zand, F. Spertini, C. Daubenberger, A. E. Corcoran and M. A. Linterman (2019). "The adjuvant GLA-SE promotes human Tfh cell expansion and emergence of public TCRbeta clonotypes." J Exp Med.
Hirota, K., J. E. Turner, M. Villa, J. H. Duarte, J. Demengeot, O. M. Steinmetz and B. Stockinger (2013). "Plasticity of Th17 cells in Peyer's patches is responsible for the induction of T cell-dependent IgA responses." Nat Immunol **14**(4): 372-379.
Iyer, S. S., S. Gangadhara, B. Victor, R. Gomez, R. Basu, J. J. Hong, C. Labranche, D. C. Montefiori, F. Villinger, B. Moss and R. R. Amara (2015). "Codelivery of Envelope Protein in Alum with MVA Vaccine Induces CXCR3-Biased CXCR5+ and CXCR5- CD4 T Cell Responses in Rhesus Macaques." J Immunol **195**(3): 994-1005.
Kumar, P., K. Chen and J. K. Kolls (2013). "Th17 cell based vaccines in mucosal immunity." Curr Opin Immunol **25**(3): 373-380.

Lê, S., J. Josse and F. Husson (2008). "FactoMineR: An R Package for Multivariate Analysis." Journal of Statistical Software **25**(1): 1 - 18.

Liao, Y., G. K. Smyth and W. Shi (2013). "featureCounts: an efficient general purpose program for assigning sequence reads to genomic features." Bioinformatics **30**(7): 923-930.

Lin, L., G. Finak, K. Ushey, C. Seshadri, T. R. Hawn, N. Frahm, T. J. Scriba, H. Mahomed, W. Hanekom, P.-A. Bart, G. Pantaleo, G. D. Tomaras, S. Rerks-Ngarm, J. Kaewkungwal, S. Nitayaphan, P. Pitisuttithum, N. L. Michael, J. H. Kim, M. L. Robb, R. J. O'Connell, N. Karasavvas, P. Gilbert, S. C De Rosa, M. J. McElrath and R. Gottardo (2015). "COMPASS identifies T-cell subsets correlated with clinical outcomes." Nature Biotechnology **33**(6): 610-616.

Love, M. I., W. Huber and S. Anders (2014). "Moderated estimation of fold change and dispersion for RNA-seq data with DESeq2." Genome Biology **15**(12): 550.

Martinez-Lopez, M., S. Iborra, R. Conde-Garrosa, A. Mastrangelo, C. Danne, E. R. Mann, D. M. Reid, V. Gaboriau-Routhiau, M. Chaparro, M. P. Lorenzo, L. Minnerup, P. Saz-Leal, E. Slack, B. Kemp, J. P. Gisbert, A. Dzionek, M. J. Robinson, F. J. Ruperez, N. Cerf-Bensussan, G. D. Brown, D. Bernardo, S. LeibundGut-Landmann and D. Sancho (2019). "Microbiota Sensing by Mincle-Syk Axis in Dendritic Cells Regulates Interleukin-17 and -22 Production and Promotes Intestinal Barrier Integrity." Immunity **50**(2): 446-461 e449.

McCausland, M. M., I. Yusuf, H. Tran, N. Ono, Y. Yanagi and S. Crotty (2007). "SAP regulation of follicular helper CD4 T cell development and humoral immunity is independent of SLAM and Fyn kinase." J Immunol **178**(2): 817-828.

Merritt, C. R., G. T. Ong, S. E. Church, K. Barker, P. Danaher, G. Geiss, M. Hoang, J. Jung, Y. Liang, J. McKay-Fleisch, K. Nguyen, Z. Norgaard, K. Sorg, I. Sprague, C. Warren, S. Warren, P. J. Webster, Z. Zhou, D. R. Zollinger, D. L. Dunaway, G. B. Mills and J. M. Beechem (2020). "Multiplex digital spatial profiling of proteins and RNA in fixed tissue." Nature Biotechnology **38**(5): 586-599.

Mitsdoerffer, M., Y. Lee, A. Jager, H. J. Kim, T. Korn, J. K. Kolls, H. Cantor, E. Bettelli and V. K. Kuchroo (2010). "Proinflammatory T helper type 17 cells are effective B-cell helpers." Proc Natl Acad Sci U S A **107**(32): 14292-14297.

Morita, R., N. Schmitt, S. E. Bentebibel, R. Ranganathan, L. Bourdery, G. Zurawski, E. Foucat, M. Dullaers, S. Oh, N. Sabzghabaei, E. M. Lavecchio, M. Punaro, V. Pascual, J. Banchereau and H. Ueno (2011). "Human blood CXCR5(+)CD4(+) T cells are counterparts of T follicular cells and contain specific subsets that differentially support antibody secretion." Immunity **34**(1): 108-121.

Moyron-Quiroz, J. E., J. Rangel-Moreno, K. Kusser, L. Hartson, F. Sprague, S. Goodrich, D. L. Woodland, F. E. Lund and T. D. Randall (2004). "Role of inducible bronchus associated lymphoid tissue (iBALT) in respiratory immunity." Nat Med **10**(9): 927-934.

Olatunde, A. C., J. S. Hale and T. J. Lamb (2021). "Cytokine-skewed Tfh cells: functional consequences for B cell help." Trends Immunol **42**(6): 536-550.

Ovsyannikova, I. G., N. Dhiman, R. M. Jacobson, R. A. Vierkant and G. A. Poland (2003). "Frequency of measles virus-specific CD4+ and CD8+ T cells in subjects seronegative or highly seropositive for measles vaccine." Clin Diagn Lab Immunol **10**(3): 411-416.

Ovsyannikova, I. G., K. C. Reid, R. M. Jacobson, A. L. Oberg, G. G. Klee and G. A. Poland (2003). "Cytokine production patterns and antibody response to measles vaccine." Vaccine **21**(25-26): 3946-3953.

Pedersen, G. K., P. Andersen and D. Christensen (2018). "Immunocorrelates of CAF family adjuvants." Semin Immunol **39**: 4-13.

Pedersen, G. K., K. Wørzner, P. Andersen and D. Christensen (2020). "Vaccine Adjuvants Differentially Affect Kinetics of Antibody and Germinal Center Responses." Frontiers in Immunology **11**.

Rao, M., S. Onkar, K. K. Peachman, Y. White, H. V. Trinh, O. Jobe, Y. Zhou, P. Dawson, M. A. Eller, G. R. Matyas and C. R. Alving (2018). "Liposome-Encapsulated Human Immunodeficiency Virus-1 gp120 Induces Potent V1V2-Specific Antibodies in Humans." J Infect Dis **218**(10): 1541-1550.

Slifka, M. K., R. Antia, J. K. Whitmire and R. Ahmed (1998). "Humoral immunity due to long-lived plasma cells." Immunity **8**(3): 363-372.

Subramanian, A., P. Tamayo, V. K. Mootha, S. Mukherjee, B. L. Ebert, M. A. Gillette, A. Paulovich, S. L. Pomeroy, T. R. Golub, E. S. Lander and J. P. Mesirov (2005). "Gene set enrichment analysis: a knowledge-based approach for interpreting genome-wide expression profiles." Proc Natl Acad Sci U S A **102**(43): 15545-15550.

Verma, A., B. A. Schmidt, S. R. Elizaldi, N. K. Nguyen, K. A. Walter, Z. Beck, H. V. Trinh, A. R. Dinsarapu, Y. S. Lakshmanappa, N. N. Rane, G. R. Matyas, M. Rao, X. Shen, G. D. Tomaras, C. C. LaBranche, K. A. Reimann, D. H. Foehl, J. S. Gach, D. N. Forthal, P. A. Kozlowski, R. R. Amara and S. S. Iyer (2019). "Impact of Th1 CD4 TFH skewing on Antibody Responses to an HIV-1 Vaccine in Rhesus Macaques." J Virol.

Ward, B. J. and D. E. Griffin (1993). "Changes in cytokine production after measles virus vaccination: predominant production of IL-4 suggests induction of a Th2 response." Clin Immunol Immunopathol **67**(2): 171-177.

Werninghaus, K., A. Babiak, O. Gross, C. Holscher, H. Dietrich, E. M. Agger, J. Mages, A. Mocsai, H. Schoenen, K. Finger, F. Nimmerjahn, G. D. Brown, C. Kirschning, A. Heit, P. Andersen, H. Wagner, J. Ruland and R. Lang (2009). "Adjuvanticity of a synthetic cord factor analogue for subunit Mycobacterium tuberculosis vaccination requires FcRgamma-Syk-Card9-dependent innate immune activation." J Exp Med **206**(1): 89-97.

Wørzner, K., J. Hvannastein, S. T. Schmidt, C. Foged, I. Rosenkrands, G. K. Pedersen and D. Christensen (2021). "Adsorption of protein antigen to the cationic liposome adjuvant CAF®01 is required for induction of Th1 and Th17 responses but not for antibody induction." Eur J Pharm Biopharm **165**: 293-305.

Acknowledgements

The authors are grateful to Dennis Christensen, previously at the SSI, for provision of CAF01 adjuvant for the studies. The authors are grateful to Brian Schmidt for technical assistance with the LAMV study; Wilhelm Von Morgenland and Miles Christensen and the CNPRC SAIDS team for coordination of macaque studies; Stephenie Liu at the UC Davis Genomics Resource for optimization of morphological markers for spatial profiling, and Daniel Newhouse at the Spatial Data Analysis Service (sDAS) for analysis of spatial proteomics data. We thank Robert L. Wilson for excellent technical assistance in processing secretions and measuring mucosal antibodies.

The authors acknowledge funding support from NIAID, NIH R56AI150409 (SSI) ; Duke CFAR Grant P30 AI064518 (GDT). Reagents for measurement of rhesus IgG subclasses were obtained from the NIH Nonhuman Primate Reagent Resource supported by AI126683 and OD10976.

Data and materials availability

RNA-seq dataset is accessible at GSE234813.

FIGURE LEGENDS

Figure 1. GC T_{fh}1 and GC T_{fh}17 cells recalled by measles booster. (**A**) Overview of study design; adult female rhesus macaques immunized with Live Attenuated Measles Virus vaccine (LAMV). **(B)** Serum MeV IgG kinetics measured by ELISA (filled circles, aged rhesus; open circles, young adults). **(C)** Avidity index (AI) of MeV IgG measured using chaotropic displacement ELISA with sodium thiocyanate at week 20 and week 0 in serum. **(D)** Representative flow cytometry plots showing $ICOS^+Ki\text{-}67^+$ circulating (c)Tfh cells in blood at day 0 and day 7 post LAMV. Kinetics of $ICOS^+Ki\text{-}67^+$ cTfh cells. **(E)** Correlation between ICOS+ Ki-67+ cTfh cells at day 7 and MeV IgG at week 20. **(F)** T_h profile of cTfh cells shows induction of $CXCR3^+$ cTfh1 at day 7. **(G)** Boolean analysis (n=16) shows cTfh1 cells induced 1 week post LAMV. Overlapping pie arcs denote cTfh cells expressing multiple chemokine receptors as denoted by arc color. **(H)** Representative flow cytometry plots show $CXCR5^+$ $PD\text{-}1^{++}$ GC T_{fh} cells and histogram shows Bcl-6 expression on GC T_{fh} cells. T_h profile of GC T_{fh} cells shows expression of CXCR3 and CCR6. **(I)** Boolean analysis of GC T_{fh} cells expressing either CXCR3 or CCR6 (n=14) shows proportion of T_h1, T_h17 and T_h1/17 GC T_{fh} subsets. **(J)** Bubble plots show genes for significantly enriched pathways related to T helper differentiation on sorted CXCR5+ PD-1+/++ cells. **(K)** Gene expression on sorted CXCR5+ PD-1+/++ cells. Statistical analysis was performed using two-tailed Wilcoxon matched-pairs signed rank test (in panels B-D, F) or spearman rank correlation test (E); * $p<0.05$, ** $p \leq 0.01$, *** $p \leq 0.001$, **** $p \leq 0.0001$.

Figure 2. Induction of Robust T Cell Activation in GCs with HIV-1 Env Formulated in CAF01 and MPLA+QS-21 Adjuvants. (A) Overview of experimental design for *in-situ*

proteomics and transcriptional analysis. **(B)** Representative images of GC from FFPE sections of inguinal LN at baseline and week 2 post protein 1 immunization with HIV-Env gp140 | MPLA+QS-21; scale bar; top, 3mm, close up, 300 µm. LN sections were stained for CD20 (blue), CD3 (yellow), Ki-67 (magenta), and DNA (gray) to identify GCs. Circular ROIs (100 µm in diameter, total 60) were selected based on co-localization of CD3 with CD20+ Ki-67+ GC B cells for proteomic profiling with a 32-plex antibody cocktail. Normalized protein expression (NPE) values were calculated using three negative control IgG probes. **(C)** NPE of key lineage markers across all ROIs at BL, P1w2, and P2w3. **(D-E)** Volcano plots show proteins induced post boost in each vaccine group. **(F)** Violin plots show common proteins induced post protein boost in MPLA and CAF01 groups. **(G)** Violin plots of proteins induced with CAF01 and MPLA. **(H)** Volcano plot (left) and Violin plots (right) of proteins significantly different across HIV-1 Env gp140 MPLA+QS-21 and CAF01 regimens. Differential expression was modeled using a linear mixed-effect model to account for the sampling of multiple ROI/AOI segments per patient/tissue. Criterion of significance was nominal p value < 0.05, plots show False discovery rate (FDR).

Figure 3. T_h1 molecular programs potentiated by HIV-1 Env/MPLA+QS-21. (A) FACS purified CD95- (naive [N]) and CD95+ CD4 T cells, stimulated overnight with HIV-1 Env, were sequenced to assess transcriptional programs. (**B**) Principal component analysis (PCA) of all expressed genes shows distinct clustering of N and CD95+ cells. (**C**) Violin plots show transcripts per million (TPM) values of differentially expressed transcription factors (p adj < 0.05) in CD95+ CD4 T cells relative to naive CD4 T cells post vaccination. (**D**) Bubble plots depict DEG at P1w2 versus BL in CD95+ CD4 T cells in CAF01 (top) and MPLA (bottom). Venn Diagram of DEG genes upregulated in CD95+ and naive subsets at P1w2 relative to BL shows 45 and 333 genes exclusively upregulated in CD95+ CD4 T cells with MPLA and CAF01, respectively. (**E**) Venn diagram of significantly downregulated genes. **(F)** PCA of all expressed genes shows distinct clustering across vaccine groups at P1w2. **(G**) Heat maps depict log_2 gene

expression (transcripts per million (TPM)) for highly DEG in CD95+ cells compared to naive cells at P1w2 in MPLA; heat map in inset depicts TPM of genes represented in Cytokine-cytokine receptor interaction pathways across vaccine regimens. (**H)** Chord plot shows GO Terms enriched with corresponding upregulated genes in CD95+ CD4 T cells at P1w2 with MPLA. **(I**) Heat maps depict log_2 gene expression (TPM) for highly DEG in CD95+ cells compared to naive cells at P1w2 in CAF01; heat map in inset depicts TPM of genes represented in Cytokine-cytokine receptor interaction pathway across vaccine regimens.

Figure 4. Phenotypically and functionally specialized GC $T_{fh}1$ / $T_{fh}17$ subsets elicited with HIV-1 Env Formulated in CAF01 and MPLA+QS-21 Adjuvants. (A) Representative flow cytometry plot illustrates GC T_{fh} cells and GC T_{fh} frequencies (%CD95) show in kinetic plot to right. **(B)** Flow cytometry plot shows identification of GC $T_{fh}1$, $T_{fh}17$, and $T_{fh}1/17$ cells with (**C**) temporal kinetics expressed as %CD95+. Significance indicates differences in GC T_{fh} subsets at P1 and P2 relative to baseline. **(D)** Proportion of $T_{fh}1$, $T_{fh}17$, $T_{fh}1/7$ and CXCR3-, CCR6- GC T_{fh} cells across CAF01 and MPLA at P1w2. **(E)** Boolean analysis (n=6 each group) shows proportion of T_h1, T_h17 and $T_h1/17$ GC T_{fh} subsets. **(F-G)** Intracellular cytokine staining (ICS) analysis of T_h1, $T_{fh}17$, $T_{fh}1/17$ subsets at P1w2. **(H)** Gating strategy (left) and frequencies (right) of circulating T_{fh} (cT_{fh}) and $cT_{fh}1$ cells in whole blood at P1w0 and P1w1. **(I)** Gating strategy (left) and frequencies (right) of activated ($CD40L^+OX40^+$) cT_{fh} ($CXCR5^+$) and non-cT_{fh} CD4 T cells (CXCR5-) cells in PBMCs at P1w1. **(J)** ICS of cTfh and non-cTfh CD4 T cells following Env stimulation at P1w1 and P2w1. Data points show individual animals. Statistical analysis was performed using two-tailed Wilcoxon matched-pairs signed rank test (in panels A, C, H) or Mann-Whitney U test (in panels D; G, I-K); * $p<0.05$, ** $p \leq 0.01$.

Figure 5. Induction of persistent anti-Env IgG antibodies with HIV-1 Env/MPLA+QS-21 (A) Kinetics of HIV-1 Env IgG post protein boost (P1 and P2) across vaccine regimens measured by

ELISA against C. 1086 gp140. **(B)** Serum gp140 IgG week 30 post P2w3. (**C**) GC $T_{fh}1$ cells correlate with gp140 IgG at week 30. **(D)** Env-specific (IFN-γ^+IL-2^+) T_{fh} cells correlate with gp140 IgG at week 30. **(E-I)** Area under the curve (AUC) values of IgG temporally shown by antigens, as indicated. (**J**) Temporal and (**K**) week 8 measures of gp140-specific IgG levels relative to total IgG in rectal secretions. Data points show individual animals. Statistical analysis was performed using Mann-Whitney U test (in panels A-B, E-K), or two-tailed Spearman rank correlation test (C-D); * $p<0.05$, ** $p \leq 0.01$.

Figure 6. Induction of IgG1 subclass antibodies with greater effector functions with HIV-1 Env/MPLA+QS-21. Serum C. 1086 gp120-specific (**A)** IgG1, **(B**) IgG2 **(C)** IgG4 antibodies at P2w2. **(D-E)** Antibody-dependent phagocytosis (ADP) score at P2w8. **(F)** C. 1086 gp120-specific IgG1 correlates with ADP score. **(G)** Infectious dose 50% (ID50) titers to Tier 1A Clade C MW965.26 HIV-1 isolate at P2w2. **(H-L)** Avidity index (with sodium citrate) across vaccine regimens against specific antigens at P2w8. Data points show individual animals. Statistical analysis was performed using two-tailed Mann-Whitney U test (in panels A-E; G-L), or two-tailed Spearman rank correlation test (F); * $p<0.05$, ** $p \leq 0.01$.

Figure 7. Differentiation of GC T_{fh} Subsets initiated during the DNA Priming Phase.

(A) Experimental design of DNA immunization phase; FNA, lymph node fine needle aspirates. **(B)** Intracellular expression of Gag (2F12), surface expression of HIV-1 Env (PGT121) and IP10 and IL6 in supernatants of transfected 293T cells. **(C)** Flow cytometry plots show activated (PD-1^+Ki-67^+) cTfh cells, frequencies post DNA3 (right top); frequencies of cTfh1 cells (right bottom). **(D)** GC T_{fh} cells, **(E**) Ki-67^+ PD1^+ cells of CXCR5+ subset in lymph node. **(F**) CXCR3+ subset of Ki-67^+ PD-1^+ CXCR5^+ subset. (**G**) Ki-67+ PD-1+ T_{fh} in LN correlate with gp140 IgG at week 4 post DNA3. (**H**) Ki-67+ PD-1+ $T_{fh}1$ in LN correlate with gp140 IgG at week 4 post DNA. **(I**) gp140 IgG at week 2 post P1 correlates with gp140 IgG at week 4 post DNA3. Data points show

individual animals. Statistical analysis was performed using one-tailed Wilcoxon matched-pairs signed rank test (in panels C-F), or Spearman rank correlation test (G-I); * $p<0.05$.

S1, Supplement to Figure 1.

(**A**). Gating strategy to identify $CXCR5^+$ $OX40^+$ $CD25^+$ MeV-specific T_{fh} cells within PBMCs following stimulation with MeV antigen at Day 0 and Day 7 post LAMV. Right panel illustrates the MeV specific responses in CD4 T cells (%CD95) at weeks 0, 1, and 8 following immunization. (**B**). Flow plots illustrate gating strategy to identify cTfh cells. (**C**). Representative histograms show expression of TIGIT, CD200, CXCR3, CCR6, and CCR4 on GC Tfh cells in LN. (**D**). Sorting schematic to isolate CXCR5+ PD-1+/++ cells for RNA sequencing.

S2. Experimental design of DNA-prime/Protein-boost Clade C HIV-1 immunization.

S3, Supplement to Figure 2. Sequencing QC histograms show (**A**) Signal-to-noise ratio computed by dividing raw count values by the geometric mean of the negative IgG probes. Quality control metrics- (**B**) deduplicated reads, (**C**) percent aligned reads, **(D)** sequencing saturation. (**E)** Bubble plot shows correlation of CD20 protein expression with CD4; bubble size corresponds to PD-1 expression, color intensity, Ki-67 expression; Spearman value, two-tailed p value of 60 pairs **(F)** Bubble plot shows correlation of CD4 protein expression with 4-1BB; bubble size corresponds to ICOS expression, color intensity, STING expression; Spearman value, two-tailed p value of 60 pairs. **(G)** Heatmap plots show unsupervised hierarchical clustering of z-score values for each protein across time for each animal.

S4, Supplement to Figure 3. (A-B) QC metrics **(C)** Bar graph shows DEG genes within CD4 subsets post vaccination relative to baseline. (**D**) PCA plot of CD95+ CD4 T cell subsets at P2w3 (**E**) Bubble plots show DEG enriched in CD95+ subsets at P1w2 in CAF01 and MPLA.

GO-Terms of biological pathways differential induced in MPLA (**F**) and CAF01 (**G**) in CD95+ CD4 T cells at P1w2.

S5, Supplement to Figure 4. (A) Illustrates gating strategy to identify GC T_{fh} cells. **(B)** Frequencies of T_{fh} cells ($CD4^+CD95^+PD\text{-}1^+CXCR5^+$) (Top), $T_{fh}1$ cells ($CD4^+CD95^+PD\text{-}1^+CXCR5^+CXCR3^+$) (Middle), and $T_{fh}1/17$ cells ($CD4^+CD95^+PD\text{-}1^+CXCR5^+CXCR3^+CCR6^+$) in lymph nodes. **(C)** Intracellular cytokine staining (ICS) to identify Env-specific T_{fh} cells. (**D**) Co-expression of IL-2 and TNFa in IFNG+ versus IFNG- subsets producing IL-21. **(E)** Serum IL-21 post P1. **(F)** Gating of AIM assay

S6, Supplement to Figure 6. Serum C. 1086 gp120-specific IgG1 (grey), IgG2 (pink), and IgG4 (black) in animals (x-axis – animal IDs) P2w3

S7, Supplement to Figure 7. Frequencies of $OX40^+CD40L^+$ cTfh cells stimulated ex vivo with Gag and Env.

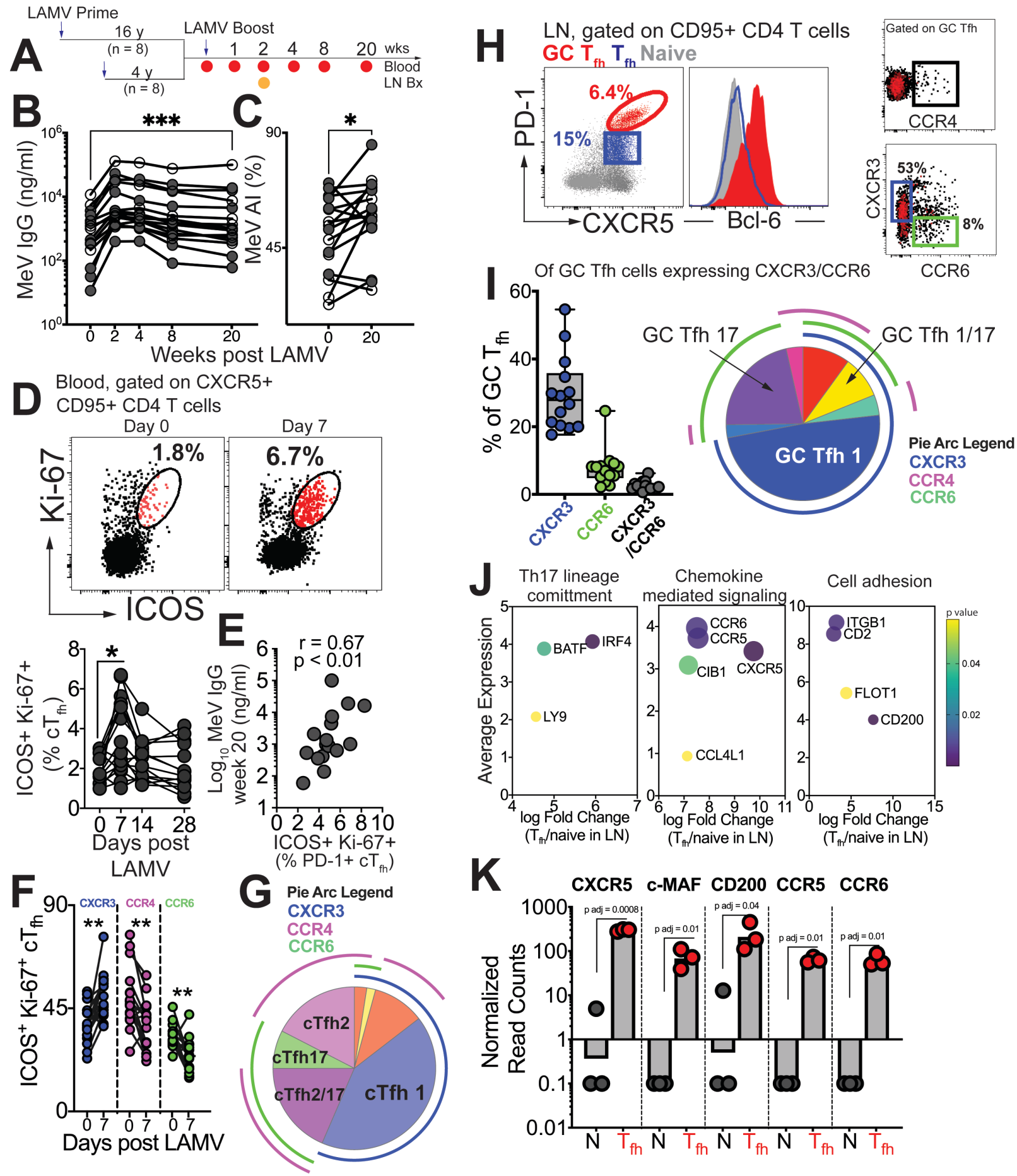
A
LAMV Prime
16 y
(n = 8)
4 y
(n = 8)
LAMV Boost
1 2 4 8 20 wks
Blood
LN Bx
B
MeV IgG (ng/ml)
Weeks post LAMV
C
MeV AI (%)
D
Blood, gated on CXCR5+
CD95+ CD4 T cells
Day 0
Day 7
1.8%
6.7%
Ki-67
ICOS
E
r = 0.67
p < 0.01
Log10 MeV IgG
week 20 (ng/ml)
ICOS+ Ki-67+
(% PD-1+ cTfh)
ICOS+ Ki-67+
(% cTfh)
Days post
LAMV
F
CXCR3
CCR4
CCR6
ICOS+ Ki-67+ cTfh
Days post LAMV
G
Pie Arc Legend
CXCR3
CCR4
CCR6
cTfh2
cTfh17
cTfh2/17
cTfh 1
H
LN, gated on CD95+ CD4 T cells
GC Tfh Tfh Naive
6.4%
15%
PD-1
CXCR5
Bcl-6
Gated on GC Tfh
CCR4
53%
8%
CXCR3
CCR6
I
Of GC Tfh cells expressing CXCR3/CCR6
% of GC Tfh
CXCR3
CCR6
CXCR3
/CCR6
GC Tfh 17
GC Tfh 1/17
GC Tfh 1
Pie Arc Legend
CXCR3
CCR4
CCR6
J
Th17 lineage
comittment
Chemokine
mediated signaling
Cell adhesion
Average Expression
BATF
IRF4
LY9
CCR6
CCR5
CIB1
CXCR5
CCL4L1
ITGB1
CD2
FLOT1
CD200
p value
log Fold Change
(Tfh/naive in LN)
K
CXCR5
c-MAF
CD200
CCR5
CCR6
Normalized
Read Counts
p adj = 0.0008
p adj = 0.01
p adj = 0.04
p adj = 0.01
p adj = 0.01
N
Tfh

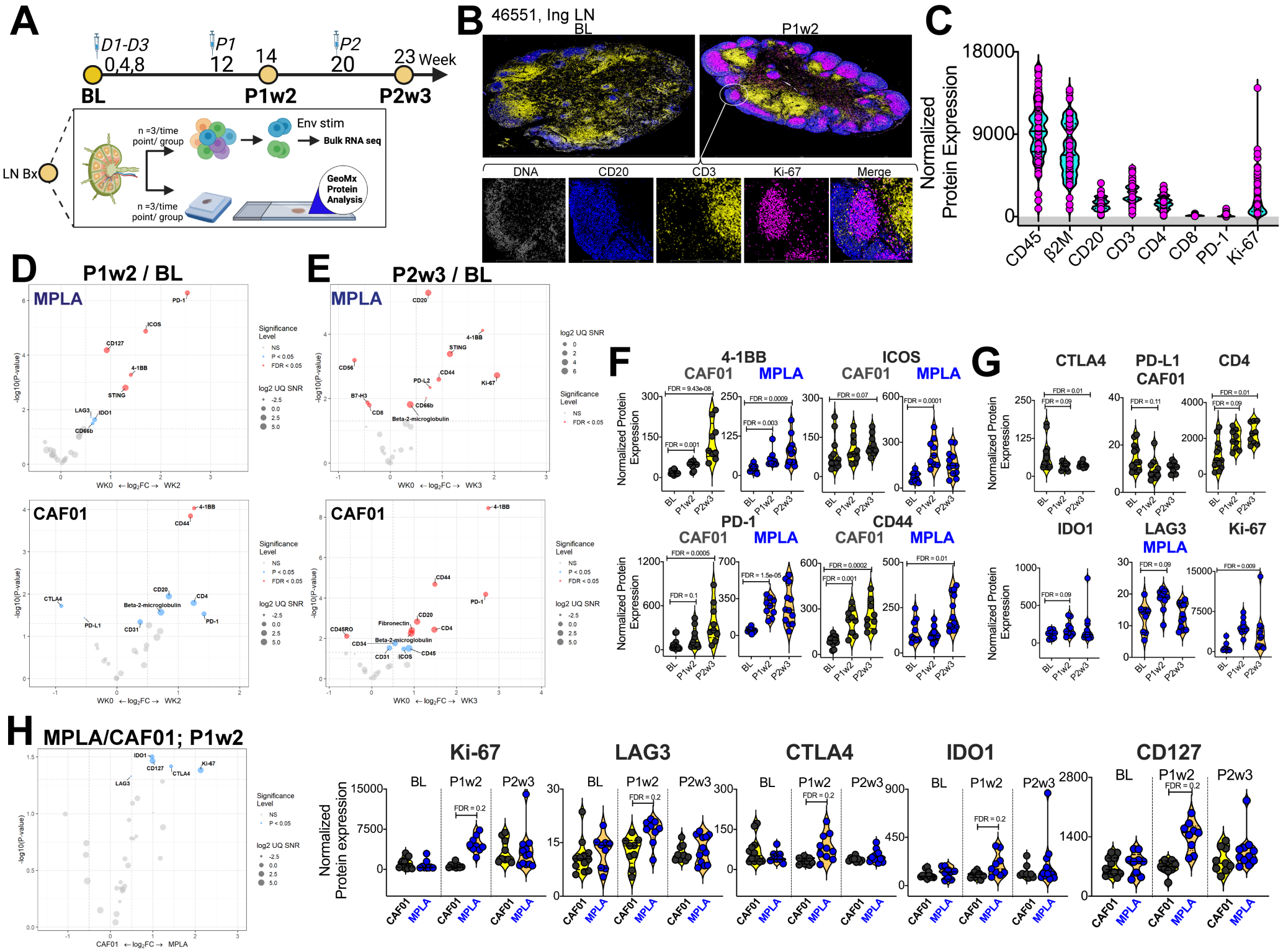
A
D1-D3
0,4,8
P1
12
14
P2
20
23 Week
BL
P1w2
P2w3
LN Bx
n =3/time point/ group
Env stim
Bulk RNA seq
GeoMx Protein Analysis
B
46551, Ing LN
BL
P1w2
DNA
CD20
CD3
Ki-67
Merge
C
Normalized Protein Expression
18000
9000
0
CD45
β2M
CD20
CD3
CD4
CD8
PD-1
Ki-67
D
P1w2 / BL
MPLA
CAF01
E
P2w3 / BL
MPLA
CAF01
Significance Level
NS
P < 0.05
FDR < 0.05
log2 UQ SNR
-2.5
0.0
2.5
5.0
-log10(P-value)
WK0 ← log2FC → WK2
WK0 ← log2FC → WK3
F
4-1BB
ICOS
PD-1
CD44
CAF01
MPLA
Normalized Protein Expression
BL
P1w2
P2w3
G
CTLA4
PD-L1
CD4
IDO1
LAG3
Ki-67
H
MPLA/CAF01; P1w2
CAF01 ← log2FC → MPLA
Ki-67
LAG3
CTLA4
IDO1
CD127
Normalized Protein expression
BL
P1w2
P2w3
CAF01
MPLA
FDR = 0.2

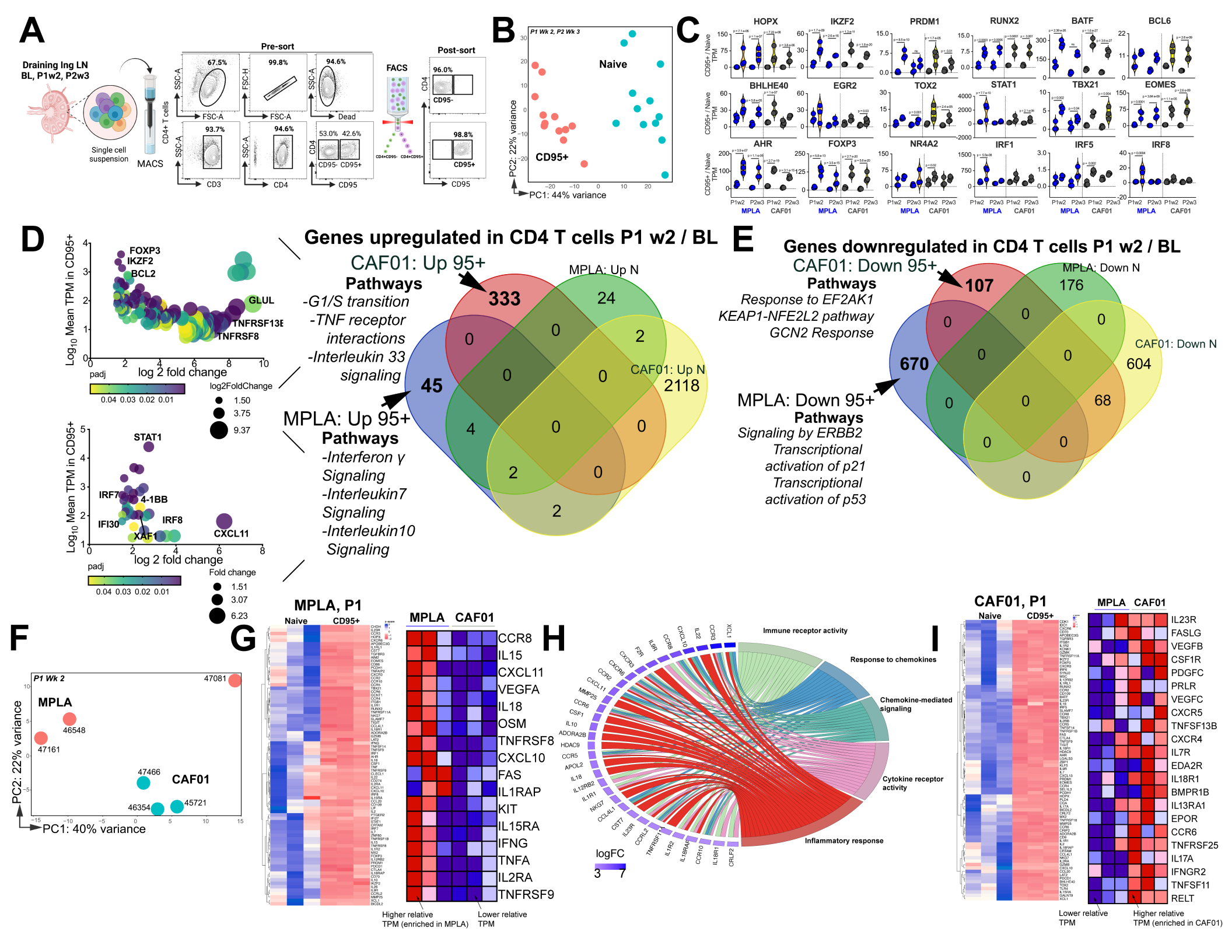
A
Draining Ing LN
BL, P1w2, P2w3
Single cell suspension
MACS
Pre-sort
Post-sort
FACS
CD4+ T cells
67.5%
99.8%
94.6%
93.7%
94.6%
53.0%
42.6%
96.0%
98.8%
SSC-A
FSC-A
FSC-H
Dead
CD3
CD4
CD95
CD95-
CD95+
B
P1 Wk 2, P2 Wk 3
Naive
CD95+
PC2: 22% variance
PC1: 44% variance
C
HOPX
IKZF2
PRDM1
RUNX2
BATF
BCL6
BHLHE40
EGR2
TOX2
STAT1
TBX21
EOMES
AHR
FOXP3
NR4A2
IRF1
IRF5
IRF8
CD95+ / Naive TPM
P1w2
P2w3
MPLA
CAF01
D
Genes upregulated in CD4 T cells P1 w2 / BL
CAF01: Up 95+
Pathways
-G1/S transition
-TNF receptor interactions
-Interleukin 33 signaling
MPLA: Up 95+
Pathways
-Interferon γ Signaling
-Interleukin7 Signaling
-Interleukin10 Signaling
MPLA: Up N
CAF01: Up N
333
24
2
45
4
2
2
0
0
0
0
0
0
0
0
0
0
2118
FOXP3
IKZF2
BCL2
GLUL
TNFRSF13B
TNFRSF8
STAT1
IRF7
4-1BB
IFI30
IRF8
XAF1
CXCL11
Log10 Mean TPM in CD95+
log 2 fold change
padj
0.04 0.03 0.02 0.01
log2FoldChange
1.50
3.75
9.37
Fold change
1.51
3.07
6.23
E
Genes downregulated in CD4 T cells P1 w2 / BL
CAF01: Down 95+
Pathways
Response to EF2AK1
KEAP1-NFE2L2 pathway
GCN2 Response
MPLA: Down 95+
Pathways
Signaling by ERBB2
Transcriptional activation of p21
Transcriptional activation of p53
MPLA: Down N
CAF01: Down N
107
176
670
604
68
0
0
0
0
0
0
0
0
0
0
0
F
P1 Wk 2
MPLA
CAF01
47081
46548
47161
47466
46354
45721
PC2: 22% variance
PC1: 40% variance
G
MPLA, P1
Naive
CD95+
MPLA
CAF01
CCR8
IL15
CXCL11
VEGFA
IL18
OSM
TNFRSF8
CXCL10
FAS
IL1RAP
KIT
IL15RA
IFNG
TNFA
IL2RA
TNFRSF9
Higher relative TPM (enriched in MPLA)
Lower relative TPM
H
Immune receptor activity
Response to chemokines
Chemokine-mediated signaling
Cytokine receptor activity
Inflammatory response
logFC
3
7
I
CAF01, P1
Naive
CD95+
MPLA
CAF01
IL23R
FASLG
VEGFB
CSF1R
PDGFC
PRLR
VEGFC
CXCR5
TNFSF13B
CXCR4
IL7R
EDA2R
IL18R1
BMPR1B
IL13RA1
EPOR
CCR6
TNFRSF25
IL17A
IFNGR2
TNFSF11
RELT
Lower relative TPM
Higher relative TPM (enriched in CAF01)

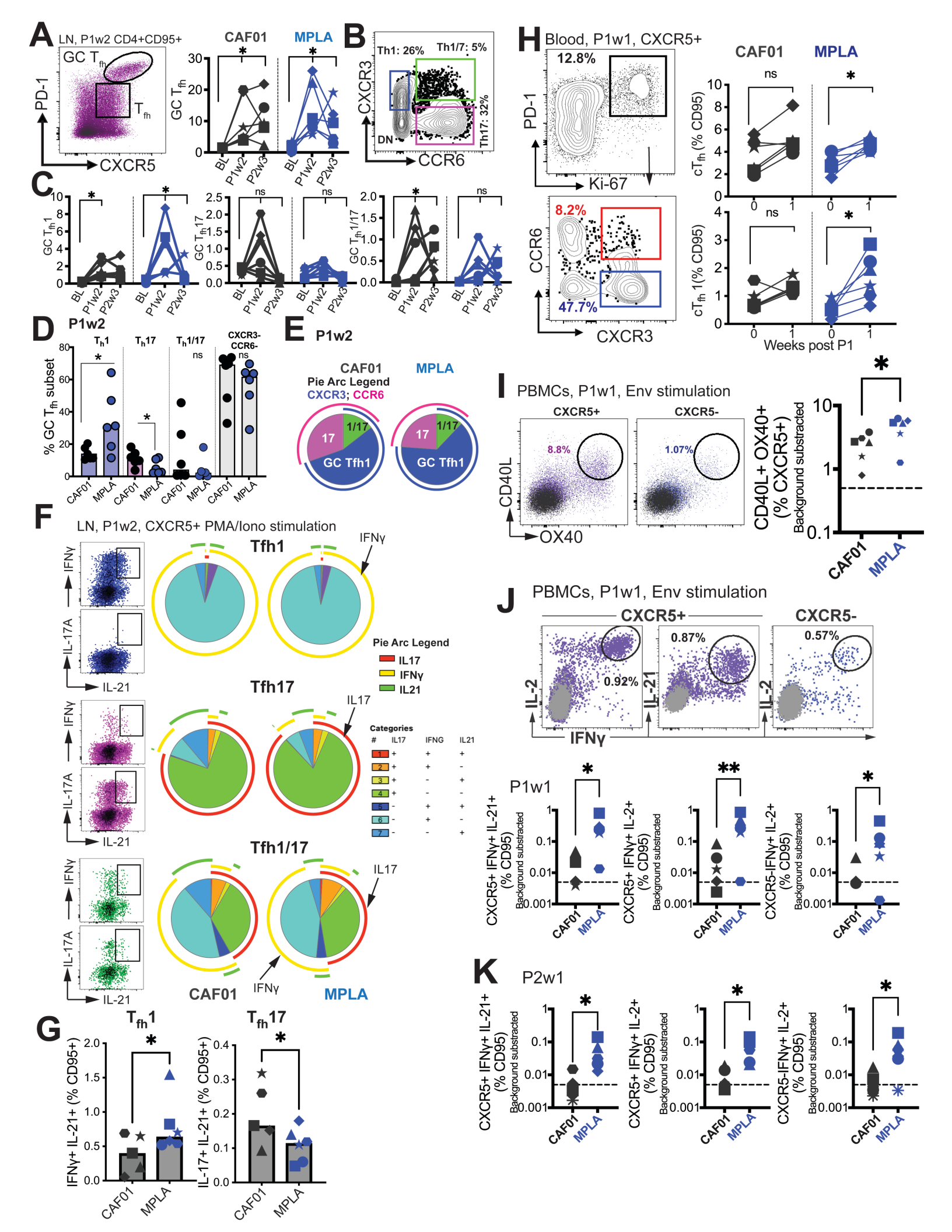
A
LN, P1w2 CD4+CD95+
GC Tfh
Tfh
PD-1
CXCR5
CAF01
MPLA
GC Tfh
BL
P1w2
P2w3
B
Th1: 26%
Th1/7: 5%
Th17: 32%
DN
CXCR3
CCR6
C
GC Th1
GC Th17
GC Th1/17
ns
D
P1w2
Th1
Th17
Th1/17
CXCR3-
CCR6-
% GC Tfh subset
E
P1w2
CAF01
MPLA
Pie Arc Legend
CXCR3; CCR6
17
1/17
GC Tfh1
F
LN, P1w2, CXCR5+ PMA/Iono stimulation
IFNγ
IL-17A
IL-21
Tfh1
Tfh17
Tfh1/17
IL17
Pie Arc Legend
IL17
IFNγ
IL21
Categories
IL17 IFNG IL21
CAF01
MPLA
G
Tfh1
Tfh17
IFNγ+ IL-21+ (% CD95+)
IL-17+ IL-21+ (% CD95+)
H
Blood, P1w1, CXCR5+
12.8%
PD-1
Ki-67
8.2%
47.7%
CCR6
CXCR3
CAF01
MPLA
cTfh (% CD95)
cTfh 1(% CD95)
Weeks post P1
I
PBMCs, P1w1, Env stimulation
CXCR5+
CXCR5-
8.8%
1.07%
CD40L
OX40
CD40L+ OX40+ (% CXCR5+)
Background substracted
J
PBMCs, P1w1, Env stimulation
CXCR5+
CXCR5-
0.92%
0.87%
0.57%
IL-2
IL-21
IFNγ
P1w1
CXCR5+ IFNγ+ IL-21+ (% CD95)
CXCR5+ IFNγ+ IL-2+ (% CD95)
CXCR5-IFNγ+ IL-2+ (% CD95)
Background substracted
K
P2w1

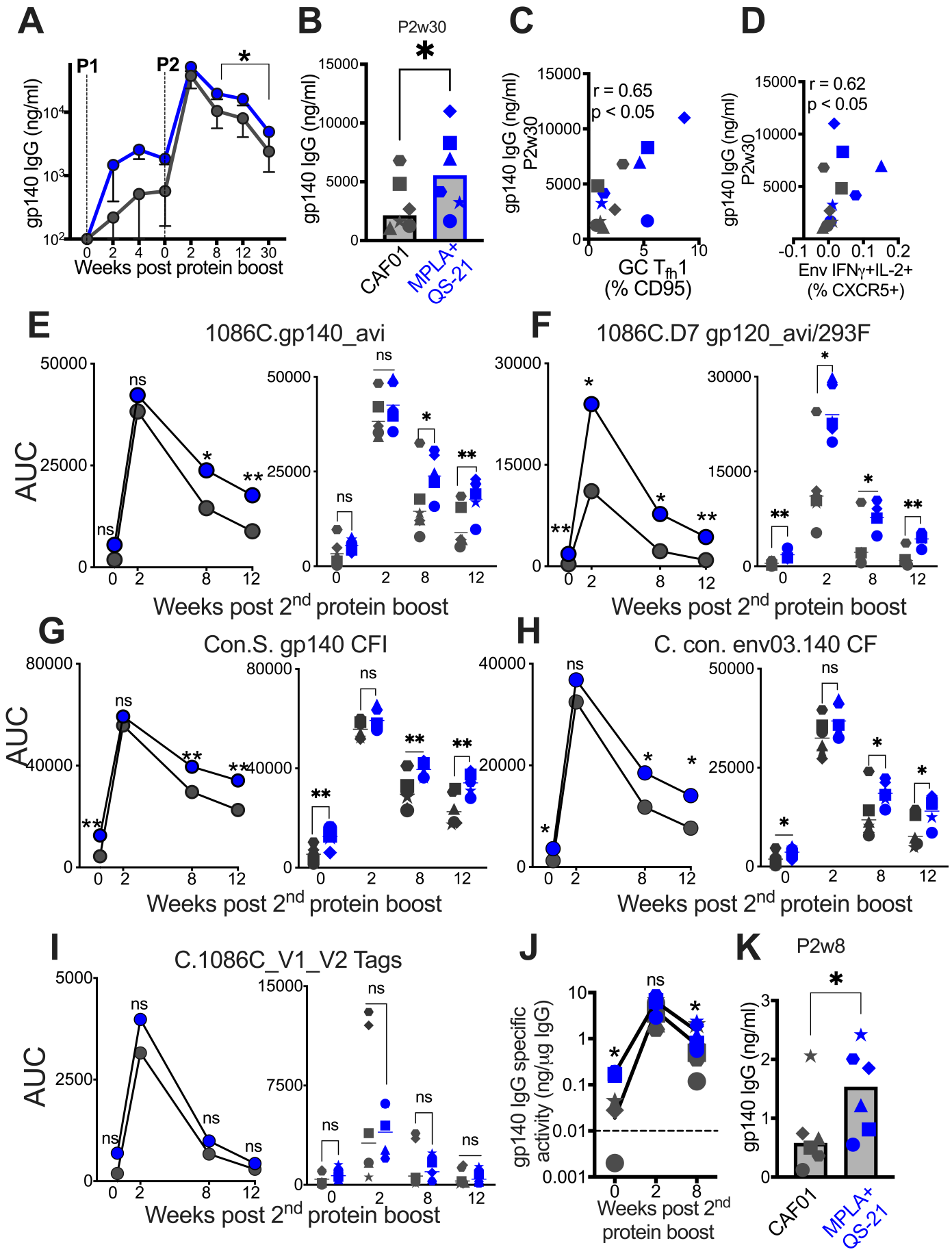
A
P1
P2
gp140 IgG (ng/ml)
Weeks post protein boost
B
P2w30
gp140 IgG (ng/ml)
CAF01
MPLA+ QS-21
C
r = 0.65
p < 0.05
gp140 IgG (ng/ml) P2w30
GC Tfh1 (% CD95)
D
r = 0.62
p < 0.05
gp140 IgG (ng/ml) P2w30
Env IFNγ+IL-2+ (% CXCR5+)
E
1086C.gp140_avi
AUC
Weeks post 2nd protein boost
F
1086C.D7 gp120_avi/293F
Weeks post 2nd protein boost
G
Con.S. gp140 CFI
AUC
Weeks post 2nd protein boost
H
C. con. env03.140 CF
Weeks post 2nd protein boost
I
C.1086C_V1_V2 Tags
AUC
Weeks post 2nd protein boost
J
gp140 IgG specific activity (ng/µg IgG)
Weeks post 2nd protein boost
K
P2w8
gp140 IgG (ng/ml)
CAF01
MPLA+ QS-21

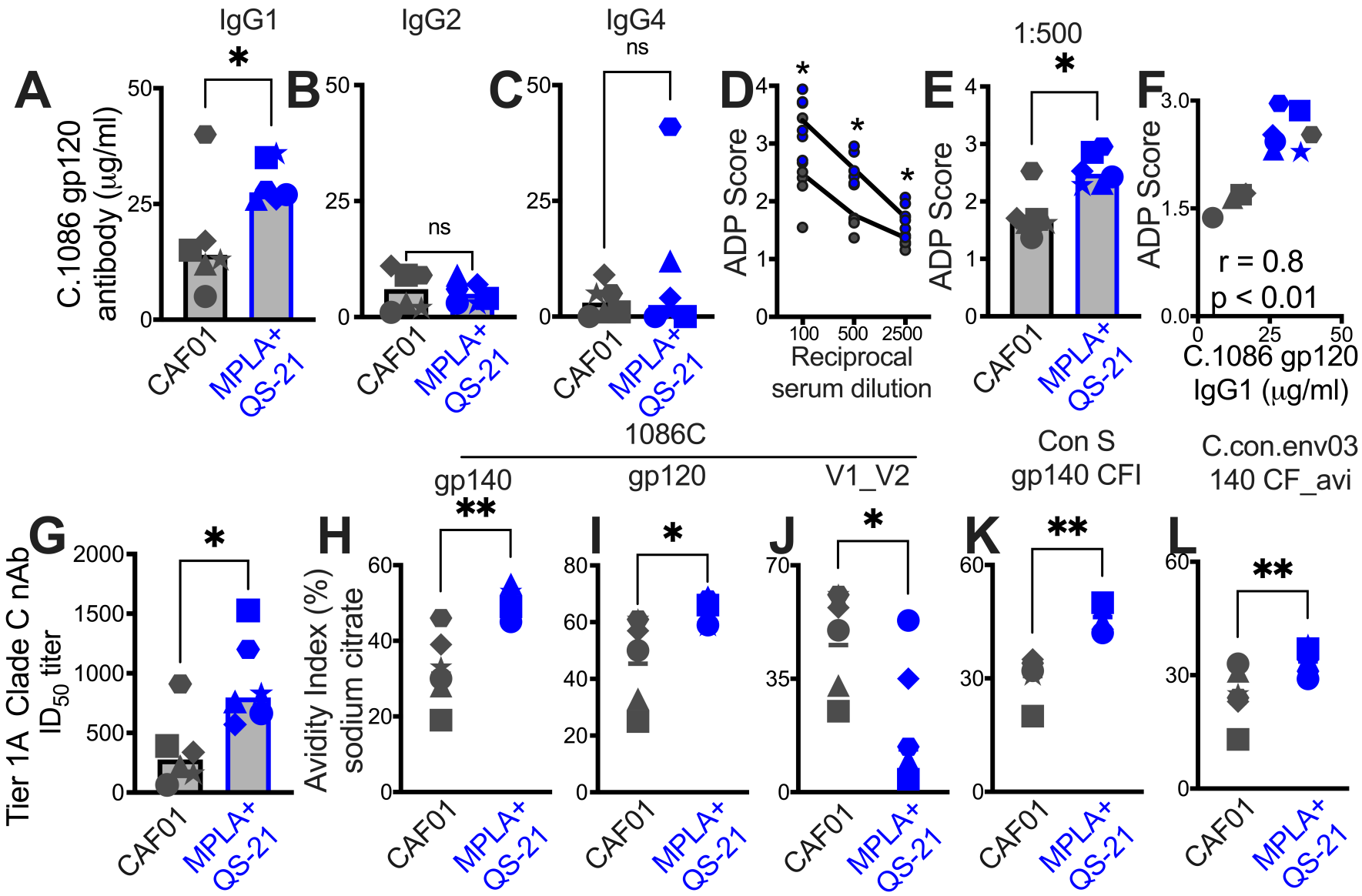
A
IgG1
C.1086 gp120 antibody (μg/ml)
CAF01
MPLA+ QS-21
B
IgG2
ns
C
IgG4
ns
D
ADP Score
Reciprocal serum dilution
E
1:500
ADP Score
F
ADP Score
r = 0.8
p < 0.01
C.1086 gp120 IgG1 (μg/ml)
1086C
gp140
gp120
V1_V2
Con S gp140 CFI
C.con.env03 140 CF_avi
G
Tier 1A Clade C nAb ID50 titer
H
Avidity Index (%) sodium citrate
I
J
K
L

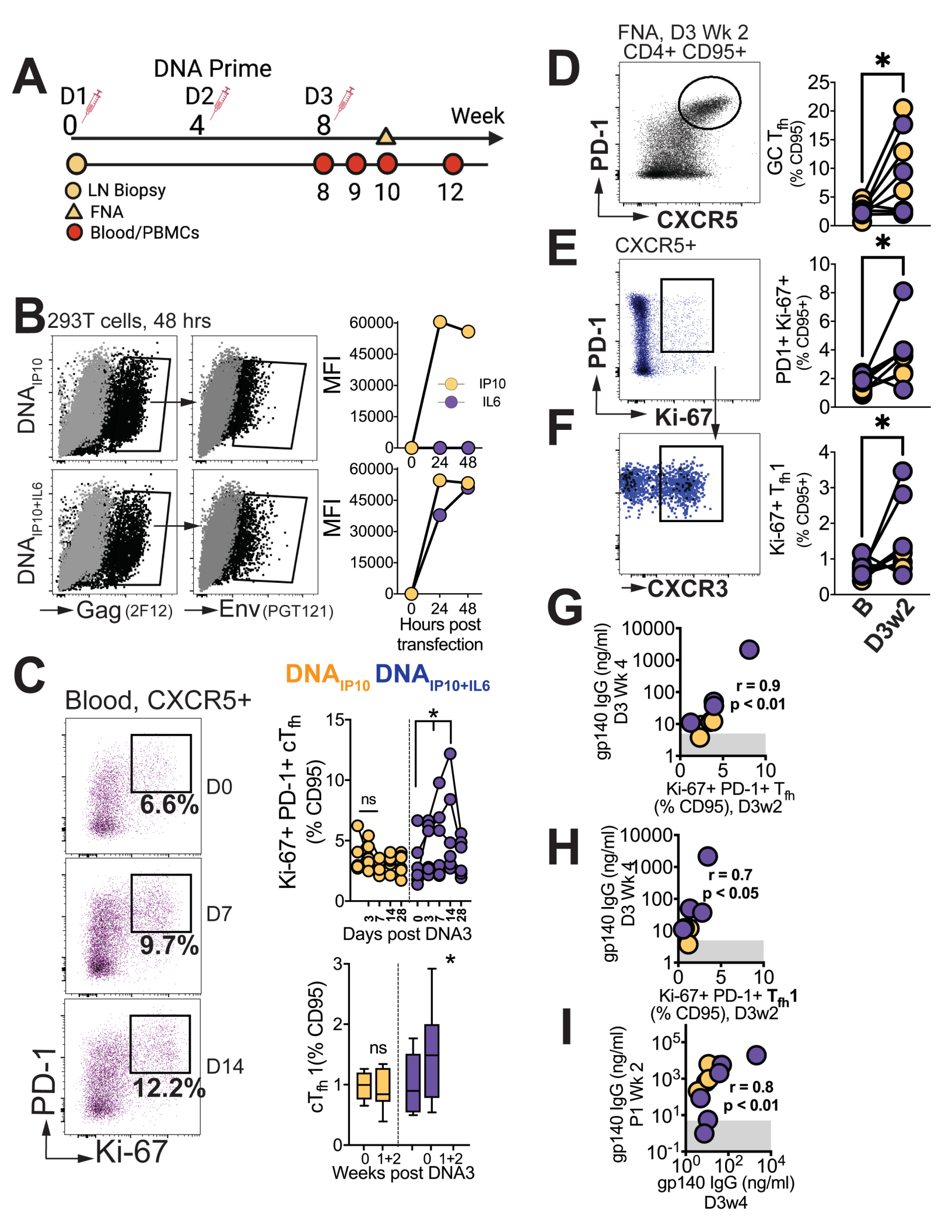
A
DNA Prime
D1
D2
D3
0
4
8
Week
LN Biopsy
FNA
Blood/PBMCs
8 9 10 12
B
293T cells, 48 hrs
DNA IP10
DNA IP10+IL6
Gag (2F12)
Env (PGT121)
MFI
IP10
IL6
0 24 48
Hours post transfection
C
Blood, CXCR5+
D0
6.6%
D7
9.7%
D14
12.2%
PD-1
Ki-67
DNA IP10
DNA IP10+IL6
Ki-67+ PD-1+ cTfh (% CD95)
ns
*
Days post DNA3
cTfh 1(% CD95)
Weeks post DNA3
D
FNA, D3 Wk 2
CD4+ CD95+
PD-1
CXCR5
GC Tfh (% CD95)
E
CXCR5+
PD-1
Ki-67
PD1+ Ki-67+ (% CD95+)
F
CXCR3
Ki-67+ Tfh1 (% CD95+)
B
D3w2
G
gp140 IgG (ng/ml) D3 Wk 4
r = 0.9
p < 0.01
Ki-67+ PD-1+ Tfh (% CD95), D3w2
H
gp140 IgG (ng/ml) D3 Wk 4
r = 0.7
p < 0.05
Ki-67+ PD-1+ Tfh1 (% CD95), D3w2
I
gp140 IgG (ng/ml) P1 Wk 2
r = 0.8
p < 0.01
gp140 IgG (ng/ml) D3w4

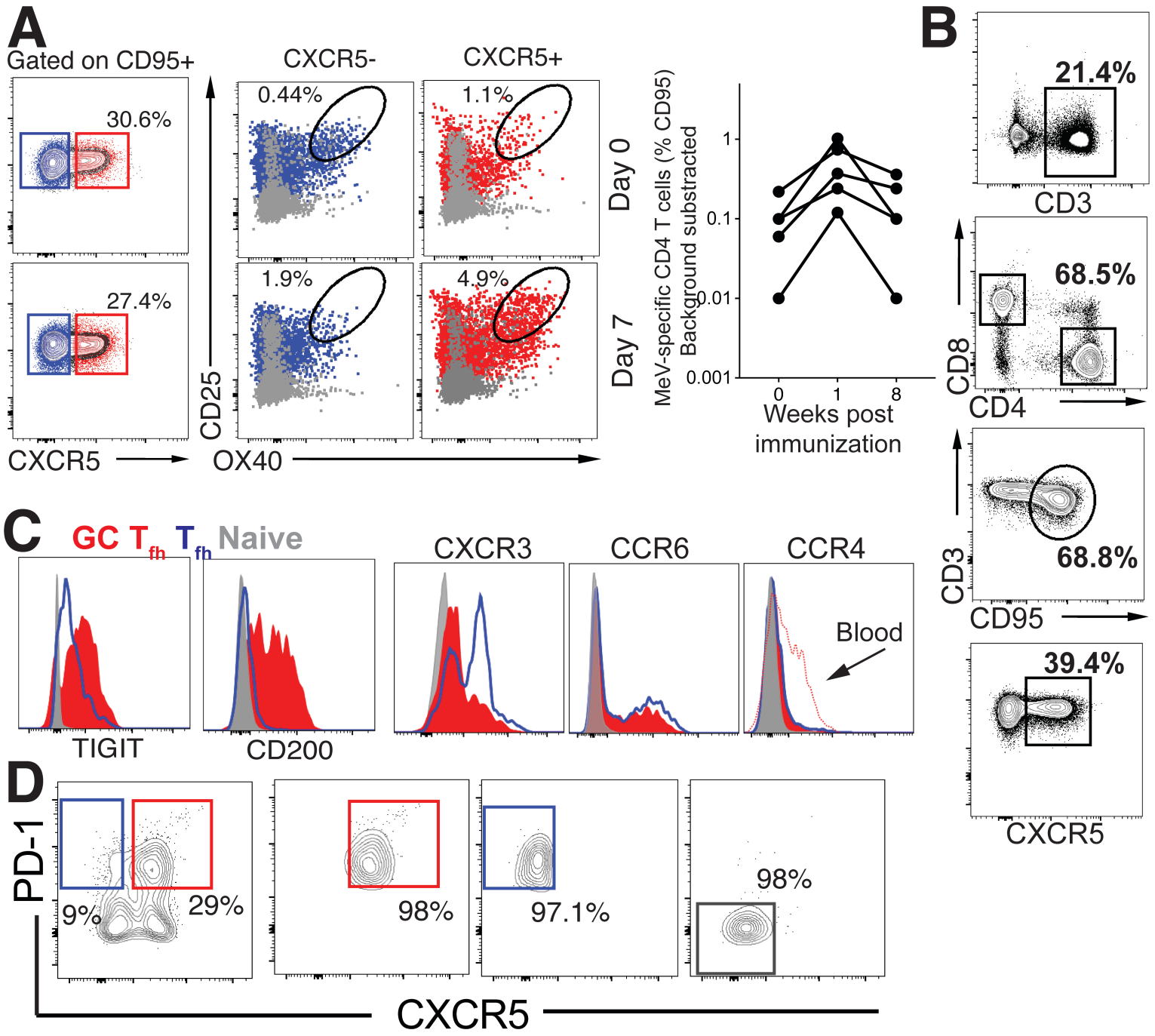
A
Gated on CD95+
CXCR5-
CXCR5+
30.6%
0.44%
1.1%
27.4%
1.9%
4.9%
Day 0
Day 7
CD25
CXCR5
OX40
MeV-specific CD4 T cells (% CD95 Background substracted)
1
0.1
0.01
0.001
0
1
8
Weeks post immunization
B
21.4%
CD3
68.5%
CD8
CD4
68.8%
CD3
CD95
39.4%
CXCR5
C
GC Tfh
Tfh
Naive
TIGIT
CD200
CXCR3
CCR6
CCR4
Blood
D
PD-1
9%
29%
98%
97.1%
98%
CXCR5

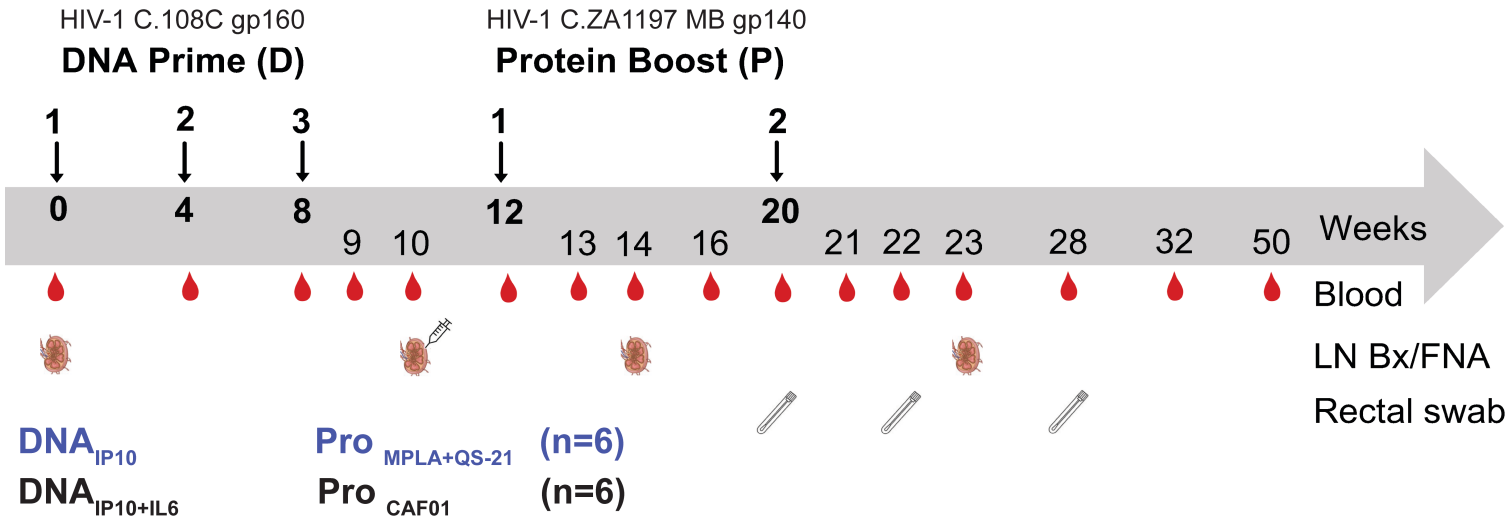
HIV-1 C.108C gp160
DNA Prime (D)
HIV-1 C.ZA1197 MB gp140
Protein Boost (P)
1
2
3
1
2
0
4
8
9
10
12
13
14
16
20
21
22
23
28
32
50
Weeks
Blood
LN Bx/FNA
Rectal swab
DNA IP10
DNA IP10+IL6
Pro MPLA+QS-21 (n=6)
Pro CAF01 (n=6)

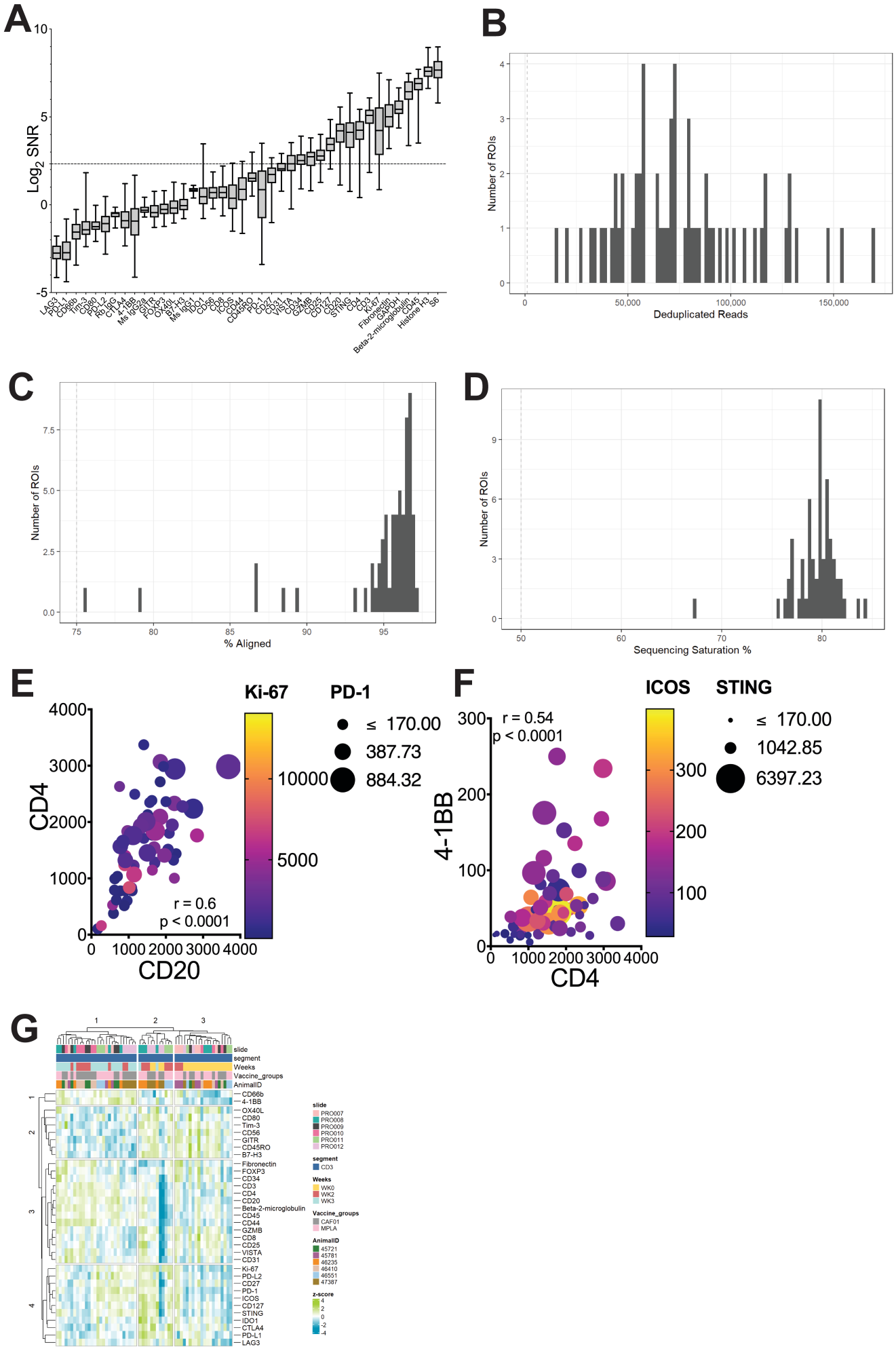
A
Log2 SNR
10
5
0
-5
LAG3
PD-L1
CD66b
Tim-3
CD80
PD-L2
Rb IgG
CTLA4
4-1BB
Ms IgG2a
GITR
FOXP3
OX40L
B7-H3
Ms IgG1
IDO1
CD56
CD8
ICOS
CD44
CD45RO
PD-1
CD27
CD31
VISTA
CD34
GZMB
CD25
CD127
CD20
STING
CD4
Ki-67
Fibronectin
GAPDH
Beta-2-microglobulin
CD45
Histone H3
S6
B
Number of ROIs
Deduplicated Reads
0
50,000
100,000
150,000
C
Number of ROIs
% Aligned
75
80
85
90
95
D
Number of ROIs
Sequencing Saturation %
50
60
70
80
E
Ki-67
PD-1
≤ 170.00
387.73
884.32
CD4
CD20
r = 0.6
p < 0.0001
F
ICOS
STING
≤ 170.00
1042.85
6397.23
r = 0.54
p < 0.0001
4-1BB
CD4
G
slide
segment
Weeks
Vaccine_groups
AnimalID
CD66b
4-1BB
OX40L
CD80
Tim-3
CD56
GITR
CD45RO
B7-H3
Fibronectin
FOXP3
CD34
CD3
CD4
CD20
Beta-2-microglobulin
CD45
CD44
GZMB
CD8
CD25
VISTA
CD31
Ki-67
PD-L2
CD27
PD-1
ICOS
CD127
STING
IDO1
CTLA4
PD-L1
LAG3
slide
PRO007
PRO008
PRO009
PRO010
PRO011
PRO012
segment
CD3
Weeks
WK0
WK2
WK3
Vaccine_groups
CAF01
MPLA
AnimalID
45721
45781
46235
46410
46551
47387
z-score

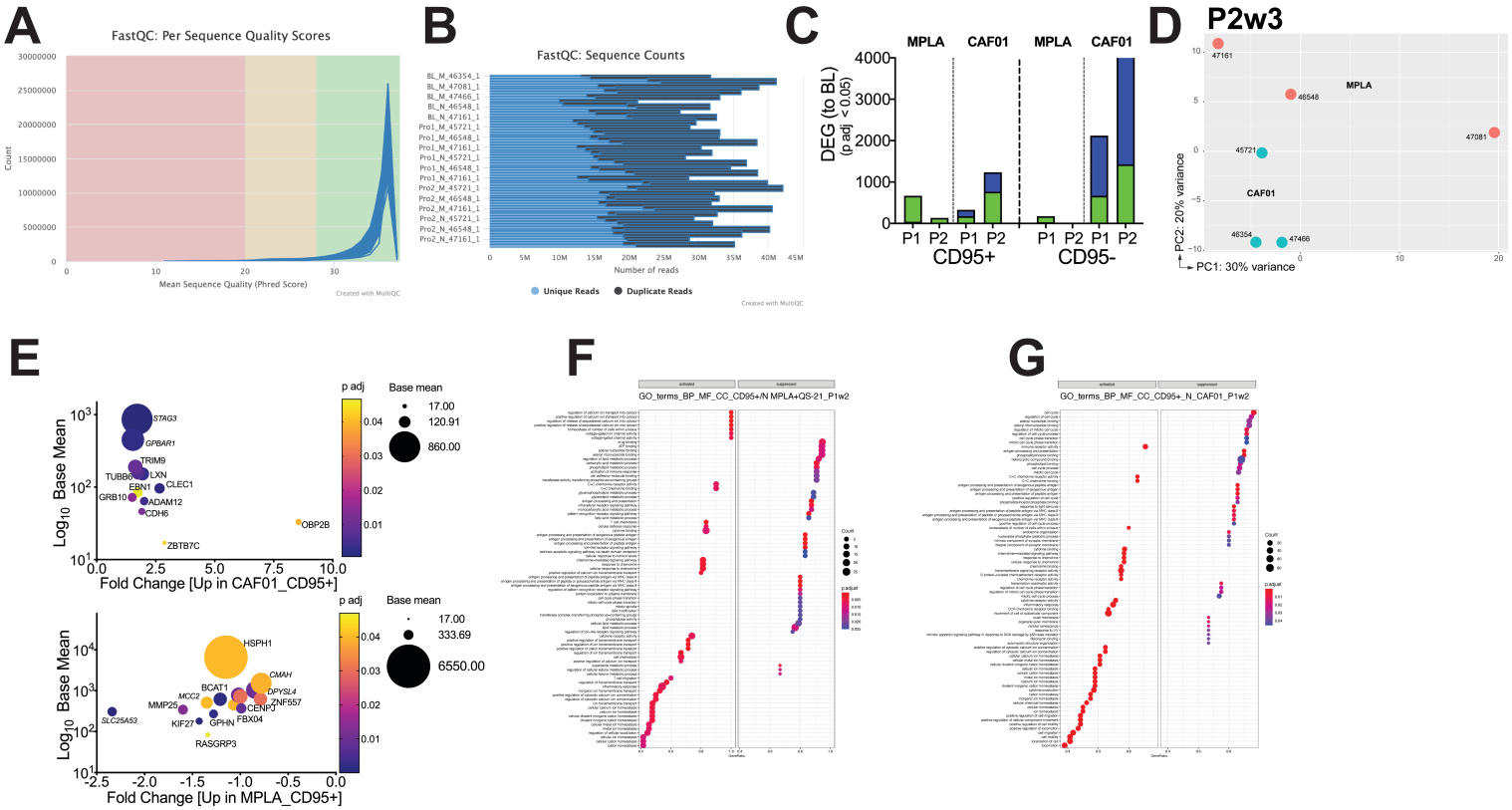
A
FastQC: Per Sequence Quality Scores
Count
Mean Sequence Quality (Phred Score)
Created with MultiQC
B
FastQC: Sequence Counts
Number of reads
Unique Reads
Duplicate Reads
Created with MultiQC
C
MPLA
CAF01
MPLA
CAF01
DEG (to BL)
(p adj < 0.05)
P1 P2 P1 P2
CD95+
P1 P2 P1 P2
CD95-
D
P2w3
MPLA
CAF01
PC2: 20% variance
PC1: 30% variance
E
p adj
Base mean
Log10 Base Mean
Fold Change [Up in CAF01_CD95+]
Fold Change [Up in MPLA_CD95+]
F
GO_terms_BP_MF_CC_CD95+/N MPLA+QS-21_P1w2
G
GO_terms_BP_MF_CC_CD95+_N_CAF01_P1w2

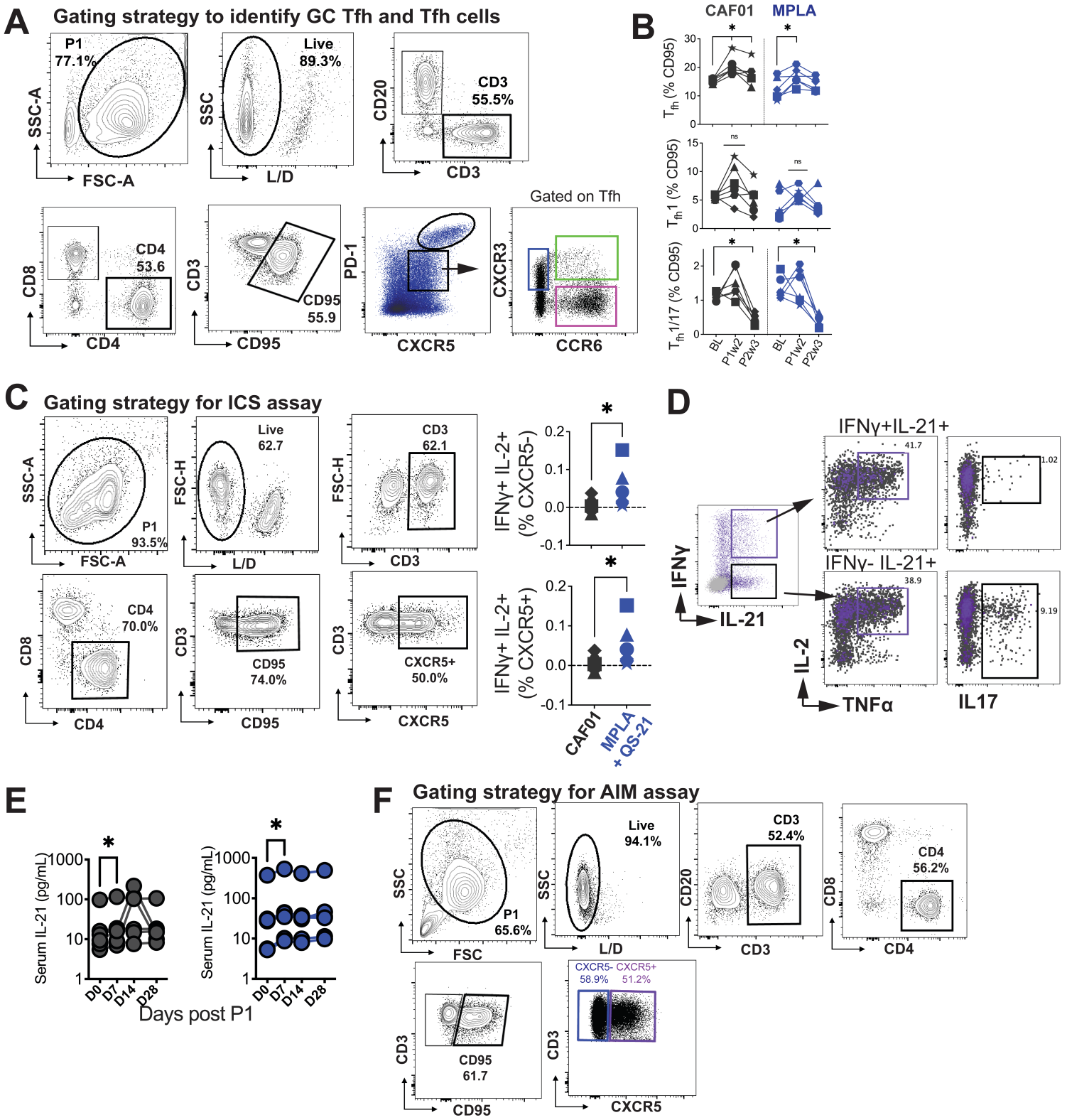
A
Gating strategy to identify GC Tfh and Tfh cells
P1
77.1%
SSC-A
FSC-A
Live
89.3%
SSC
L/D
CD3
55.5%
CD20
CD3
CD4
53.6
CD8
CD4
CD3
CD95
55.9
CD95
PD-1
CXCR5
Gated on Tfh
CXCR3
CCR6
B
CAF01
MPLA
Tfh (% CD95)
Tfh1 (% CD95)
Tfh1/17 (% CD95)
ns
BL
P1w2
P2w3
C
Gating strategy for ICS assay
P1
93.5%
Live
62.7
CD3
62.1
CD4
70.0%
CD95
74.0%
CXCR5+
50.0%
IFNγ+ IL-2+
(% CXCR5-)
IFNγ+ IL-2+
(% CXCR5+)
CAF01
MPLA
+ QS-21
D
IFNγ+IL-21+
IFNγ- IL-21+
41.7
1.02
38.9
9.19
IFNγ
IL-21
IL-2
TNFα
IL17
E
Serum IL-21 (pg/mL)
Days post P1
D0
D7
D14
D28
F
Gating strategy for AIM assay
P1
65.6%
Live
94.1%
CD3
52.4%
CD4
56.2%
CD95
61.7
CXCR5- CXCR5+
58.9% 51.2%
CXCR5

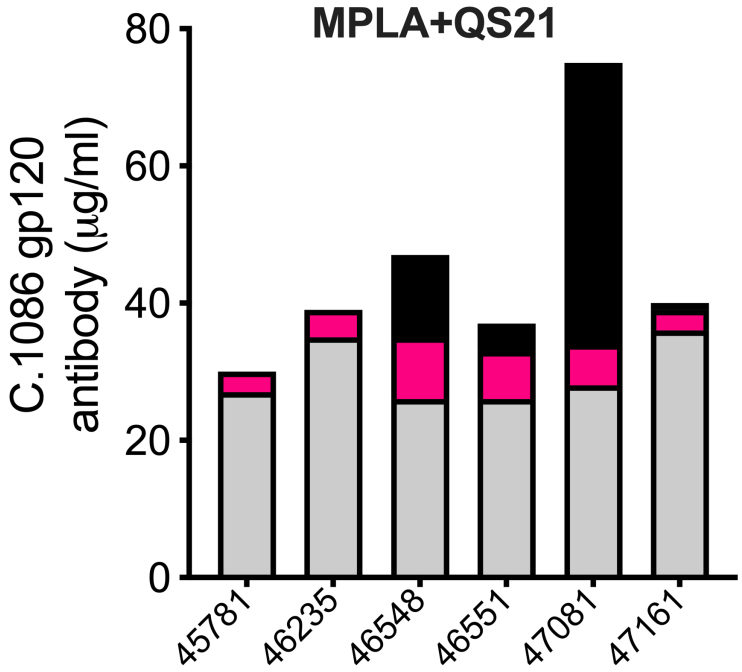

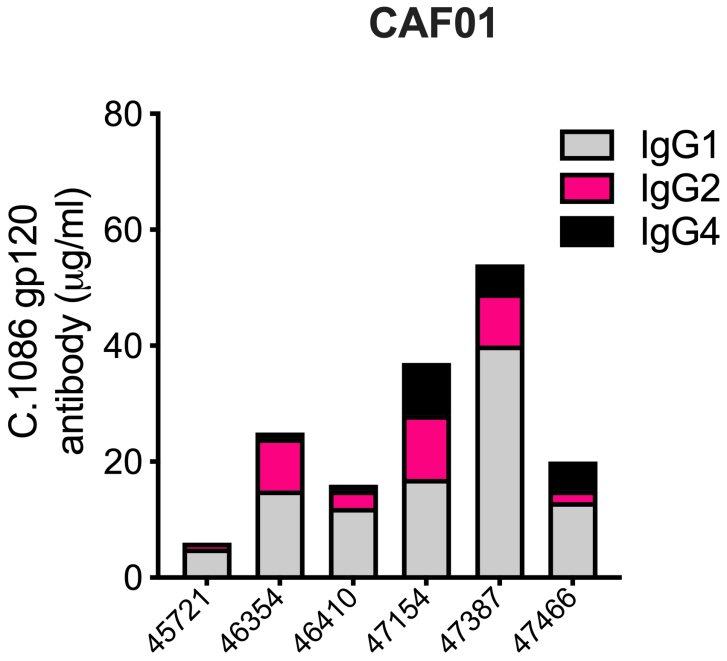

	IgG1	IgG2	IgG4
Number of values	6	6	6
Minimum	26.00	3.000	0.000
25% Percentile	26.00	3.000	0.000
Median	27.50	5.000	2.500
75% Percentile	35.25	7.500	19.25
Maximum	36.00	9.000	41.00
Range	10.00	6.000	41.00

	IgG1	IgG2	IgG4
Number of values	6	6	6
Minimum	5.000	1.000	0.000
25% Percentile	10.25	1.750	0.7500
Median	14.00	6.000	3.000
75% Percentile	22.75	9.500	6.000
Maximum	40.00	11.00	9.000
Range	35.00	10.00	9.000
Mean	17.00	5.833	3.500

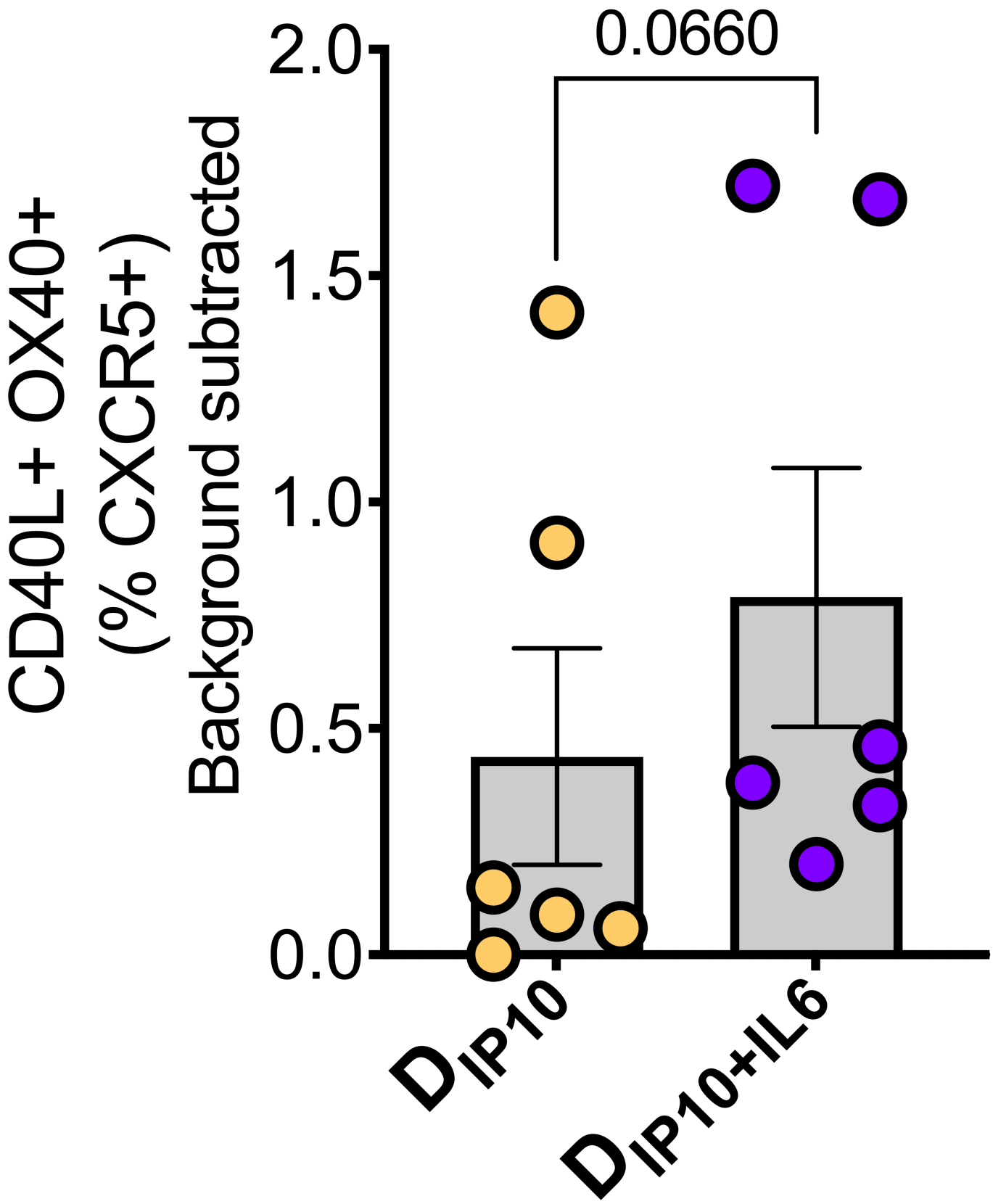
0.0660
2.0
1.5
1.0
0.5
0.0
CD40L+ OX40+
(% CXCR5+)
Background subtracted
DIP10
DIP10+IL6